공학석사 학위논문

Label-Free Particle Separation in a Viscoelastic Fluid by Using a Microfluidic Device

미세유체 시스템을 이용한 점탄성 유체 내에서의 비표지식 입자 분리

2014년 8월

서울대학교 대학원

재료공학부

김 민 정

Label-Free Particle Separation in a Viscoelastic Fluid by Using a Microfluidic Device

미세유체소자를 이용한 점탄성 유체 내에서의 비표지식 입자분리

지도 교수 윤 재 륜

이 논문을 공학석사 학위논문으로 제출함
2014 년 8월

서울대학교 대학원
재료공학부
김 민 정

김민정의 석사 학위논문을 인준함
2014년 8월

위 원 장 _____ (인)

부위원장 _____ (인)

위 원 _____ (인)

Label-Free Particle Separation in a Viscoelastic Fluid by Using a Microfluidic Device

Advisor: Jae Ryoun Youn

by

Min Jung Kim

2014

Department of Materials Science and Engineering

Graduate School

Seoul National University

ABSTRACT

A size-based microparticle separation has become indispensable in the fields of industrial production, chemical or biomedical research. Here we successfully carried out a size-based particle separation that arises from the synergistic combination between the “elasto-inertial particle focusing” and “negative magnetophoresis”. We obtained trajectories of the particle at the expanding area ($250\ \mu m \times 50\ \mu m$) by (1) calculating magnetophoretic repulsion force and drag force through the analytical modeling, (2) deriving equations of motion to solve the velocity of the particles under the laminar flow. Numerical analysis under the magnetic field was employed in order to explain a mechanism of the particle in the case of the Newtonian and viscoelastic fluid, respectively. In conclusion, we demonstrated a size-based particle separation in a microchannel with the difference between the magnetophoretic repulsion force and the drag force influenced by size. We anticipate that our platform and analysis can provide a new pathway of particle separation by using a microfluidic system.

Keywords: particle separation, elasto-inertial particle focusing, negative magnetophoresis, ferrofluid, viscoelastic fluid

Student number: 2012-23138

LIST OF FIGURES AND TABLES

volume flow rates of 50 µlh^{-1}) in the absence of the magnetic field. The image shows the distribution of 5 μm and 20μm diameter polystyrene particles at four different axial locations A-D.

Figure 4.10. Migration of polystyrene particles in viscoelastic fluid (PEO 0.4 wt% in DI water mixed with glycerol solution containing ferrofluid 10wt% at the volume flow rates of 50 µlh^{-1}) under the magnetic field. The image shows the distribution of 5 μm and 20μm diameter polystyrene particles at five different axial locations A-E.

Figure 4.11. Recovery rate at each outlet for the collected polystyrene particles after the experiment. The recovery rate defines as the ratio of the total number of particles flew for 30 s to the number of the particles corresponding to each of the particle size flew for 30 s.

Figure 4.12. Analytical modeling area.

Figure 4.13. Time-dependent change in the position of y-axis in the case of the 5 μm particles.

Figure 4.14. Time-dependent change in the position of y-axis in the case of the 20 μm particles.

Figure 4.15. Experimental results of particle trajectories with a diameter of 5 μm and 20 μm particle, respectively. Analytical modeling of particle trajectories under the magnetic field with a diameter of 5 μm and 20 μm particle, respectively.

Figure 4.16. Illustration of simulation area.

Figure 4.17. The image indicates of the migration of polystyrene particles in

CONTENTS

I. INTRODUCTION

1.1.Overview of particle separation in microfluidics

The separation of microparticles suspended in complex fluids are essential in a wide range of applications in chemical and biological research [1], such as HIV diagnostics [2] , malaria detection [3, 4] , and cancer diagnostics[5]. Conventional techniques of cell separation employ membrane-based filtering. This approach has a limitation of membrane pore size and clogging. Because of these disadvantages, new methods for particle separation have been developed [6, 7]. Recently, microfluidic systems have shown various advantages for cell separation including, (ⅰ) potential for point-of-care(POC) diagnostic in personnel; (ⅱ) cost effective; (ⅲ) high sensitivity [8-10]. Due to their advantages, developing cell separation in a micro-scale system has become increasingly important. Conventional approach for separation relies on labels to identify cells [11]. Most widely used labeling-assisted methods are fluorescence activated cell sorting (FACS) and magnetic activated cell sorting (MACS) [12]. This approach takes long time and demands complicated labeling steps. Also removing labels from the target cells is intensive [13]. Therefore their dependence of on biochemical labels for cell identification restricts their applications [14].

In contrasts, label-free separation techniques take advantages of their intrinsic properties such as size [15] , density [16], adhesion [17]. A various force field have been introduced to separate cell in a microfluidic platform, (ⅰ) magnetic; (ⅱ) electric (ⅲ) acoustic; (ⅳ) optical; (ⅴ) viscoelastic; (ⅵ) inertial [7, 18-24].

By applying one or two forces, cells can be separated on their intrinsic properties.

Recently, it has been revealed that diamagnetic particles suspended in paramagnetic fluid experience negative magentophoresis under the magnetic field [25]. That is, particle moves toward the weaker magnetic field. This can be manipulated various applications including particles trapping [26], particle separation [13, 27], and particle focusing [28, 29] .

It has been reported that the first normal stress difference (N_1) of non-Newtonian fluid generated multiple positions in the microchannel [11, 23, 30-33]. Recently, Yang et al [23] demonstrated that particles aligned at the centerline of the straight microchannel with a synergistic effect of elasticity and inertia. This phenomenon can be manipulated particle particle separation [11, 24, 34].

1.2. Objective of this study

In this paper, we report a new label-free particle separation method that arises from the synergistic combination between the elasto-inertial particle focusing effect and negative magnetophoresis.

In viscoelastic fluid, particles were aligned at the centerline of $50\,\mu m \times 50\,\mu m$ cross sectional area and negative magnetophoresis occurred at the expanding area ($250\,\mu m \times 50\,\mu m$). Therefore we conducted the size-based particle separation under the magnetic field by adjusting the ratio of viscoelastic material and paramagnetic material.

We studied trajectories of the particle at the expanding channel by (1) calculating magnetophoretic repulsion force and drag force through the analytical modeling, (2) deriving equations of motion to solve the velocity of the particles

under the laminar flow.

Numerical analysis under the magnetic field was employed in order to explain a mechanism of the particle in the case of the Newtonian and viscoelastic fluid, respectively.

II. THEORETICAL BACKGROUND

2.1. Magnetic materials

2.1.1. Definition of fundamental quantities

When a material is placed under the magnetic field, the material is magnetized. This phenomenon is described by the magnetization vector (the magnetic moment per unit volume), **M**. Since the magnetization is induced by the field, we may assume that **M** is proportional to **B**, the magnetic flux density of the applied external field. That is,

$$\mathbf{M} = \chi\mathbf{B} \tag{1}$$

The dimensionless constant, χ, is known as a magnetic susceptibility of the material.

2.1.2. Classification of magnetic materials

All materials can be classified in terms of their magnetic behavior falling into one of five categories depending on their magnetic susceptibility (table 2.1).

The two most common types of magnetism are diamagnetism and paramagnetism. For paramagnetic and diamagnetic substances, the magnetization vector, **M,** is proportional to the magnetic field, **H**.

$$\mathbf{M} = \chi\mathbf{H} \tag{2}$$

H is defined as being an alternative measure of the magnetic field, given by **H** = **B**/μ where μ is a permeability of the material surrounding the current and defines as $\mu = \mu_0(1 + \chi)$. As shown in figure 2.1, diamagnetic materials have negative susceptibility ($\chi < 0$) and paramagnetic materials have a small positive magnetic susceptibility ($\chi > 0$).

Table 2.1. Classifications of magnetic materials: five categories depending on their magnetic susceptibility.

Diamagnetism	Paramagnetism	Ferromagnetism	Ferrimagnetism	Anti-ferromagnetism

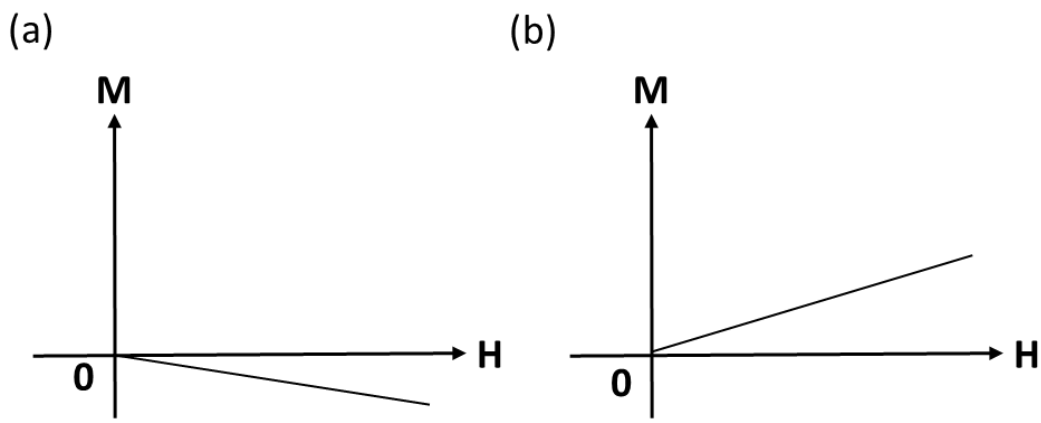

Figure 2.1. Typical effect on the magnetization, **M**, of an applied magnetic field, **H**, on (a) a diamagnetic system (b) a paramagnetic system.

2.1.2.1. Diamagnetism

Diamagnetism is a very weak form of magnetism that is non-permanent and persists only while an external field is being applied.

Diamagnetic materials have paired electrons in an atom. In other words, two electrons share the same orbital, the quantum numbers have to be different. If one of the electrons has to be upward while the other electron is downward. Whenever two electrons are paired each other in an orbital, or their total spin is "0". Therefore there is no leftover spin in an orbital and the atom is diamagnetic in the absence of the external magnetic field (figure 2.2(a)).

In the presence of an applied magnetic field, the orbiting electrons are slightly altered in their circulations, giving rise to changes in moment in a direction opposite to that of the applied field. Thus diamagnetic materials have a weak negative susceptibility ($\chi < 0$). In addition, relative magnetic permeability, μ_r, is smaller than one (i.e. $\mu_r = \mu / \mu_0 = (1 + \chi) < 1$). In other words, diamagnetic materials tend to move toward regions where the magnetic field is weak (figure 2.3(a)).

2.1.2.2. Paramagnetism

Paramagnetism is a behavior resulting from the tendency of molecular moments to align with he applied magnetic field but absence of long-range order.

Paramagnetic materials have unpaired electrons within the orbital. Because the unpaired electron does not cancel out, the orbital has a "net" spin. Therefore the entire atom get a "net" spin, it is called "paramagnetic atom". In the absence of the external magnetic field, the magnetic dipoles have no interact each other and

the orientations of these atoms are random. So the paramagnetic materials show zero magnetic moment (figure 2.2 (b)).

In the presence of an external magnetic field, the dipoles align to the applied field, resulting in a net magnetic moment in the direction of applied magnetic field. Thus paramagnetic materials have a small positive magnetic susceptibility ($\chi>0$). In addition, relative magnetic permeability, μ_r, is greater than one (i.e. $\mu_r = \mu / \mu_0 = (1 + \chi) > 1$) (figure 2.3 (b)).

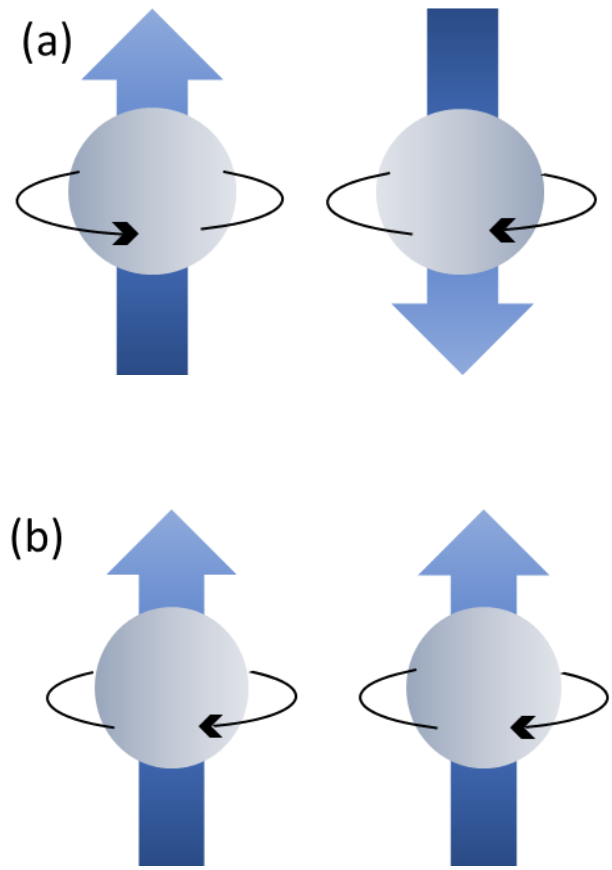

Figure 2.2. Demonstration of the magnetic moment associated with orbiting electrons (a) a diamagnetic system (b) a paramagnetic system.

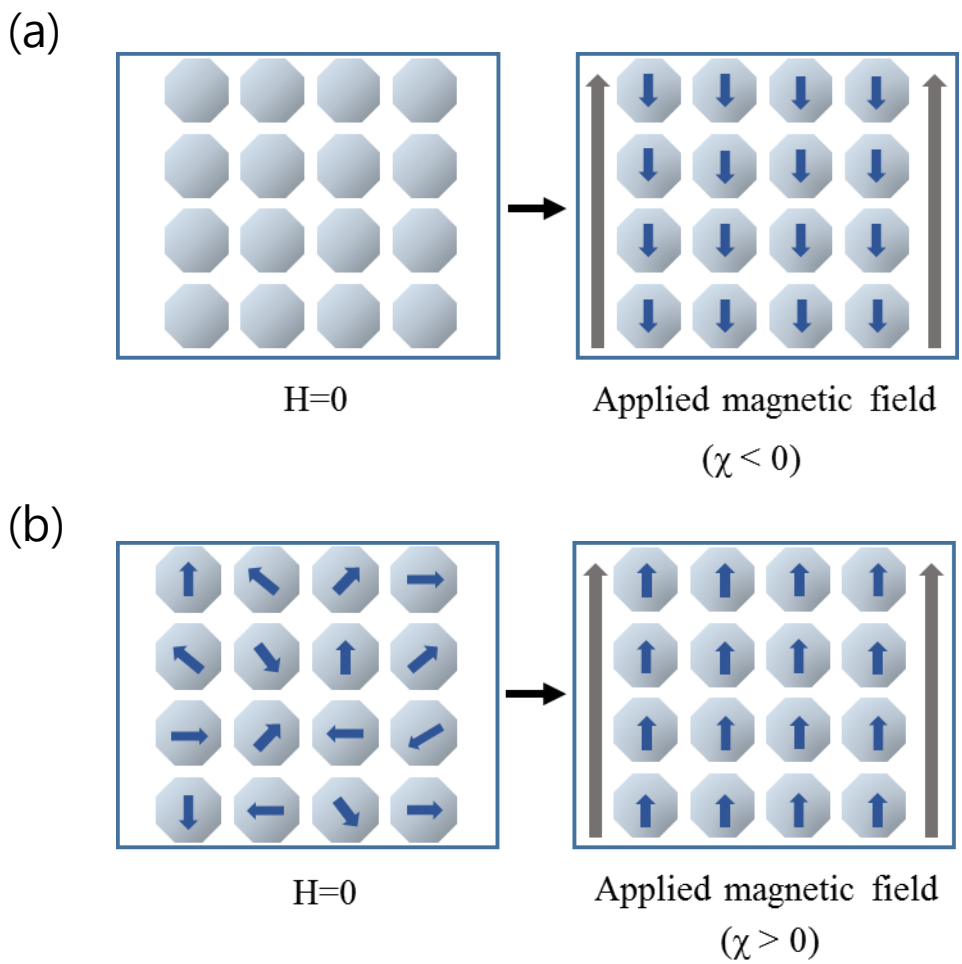

Figure 2.3. The atomic dipole configuration of (a) a diamagnetic material; in the absence of the external magnetic field, two electrons are paired each other in an orbital, therefore their total spin is "0". In the presence of an applied magnetic field, the dipoles align to opposite side of the applied field, (b) a paramagnetic material; in the absence of the external magnetic field, the paramagnetic materials show zero magnetic moment. In the presence of an external magnetic field, the dipoles align to the applied field.

2.2. Magnetophoretic repulsion force acting on the center of the diamagnetic particles

Consider a diamagnetic body immersed in a paramagnetic fluid under the magnetic field [25]. The net force acting on the diamagnetic body is defined by

$$\mathbf{F}_m = -\oint_S \left(\frac{1}{2}\mu_0 M_n^2 + \mu_0 \int_0^H M dH\right)\hat{\mathbf{n}} dS \quad (3)$$

Where S is surface that encloses the non-magnetic particle, H is magnitude of non-uniform magnetic fields, $\hat{n}$ is outward-directed unit normal vector at the particle surface, and M_n is normal component of ferrofluid magnetization adjacent to the surface S enclosing the particle. In the limit of dilute ferrofluid or intense applied magnetic field, $\frac{1}{2}M_n^2/\bar{M}H \ll 1$, where $\bar{M}$ is mean ferrofluid magnetization [35]. Applying Gauss divergence theorem, magnetophoretic repulsion force on a diamagnetic particle inside ferrofluids can be simplified to [36],

$$\mathbf{F}_m = -V_p \mu_0 (\mathbf{M_f} \cdot \nabla)\mathbf{H} \quad (4)$$

Where V_p is a volume of the diamagnetic particle, μ_0 is the permeability of free space, $\mathbf{M}_f$ is vector of the effective magnetization of the ferrofluid, and $\mathbf{H}$ is vector of the magnetic field at the non-magnetic particle center.

Magnitude of the magnetization of ferrofluid, M_f is determined using a Langevin function, $L(\alpha)$, that can be described as

$$\frac{M_f}{\phi M_d} = L(\alpha) = \coth(\alpha) - \frac{1}{\alpha} \quad (5)$$

$$\alpha = \frac{\pi d^3 \mu_0 M_d H}{6 k_B T}$$

Where ϕ is volume fraction of magnetic nanoparticles with a saturation moment

of magnetic nanoparticles, M_d, and $M_d = 4.377 \times 10^5$ A/m as calculated from the manufacturer-provided saturation magnetization of the ferrofluid $M_{sat} = 5252$ A/m. through the saturation magnetization of a ferrofluid, M_{sat}, equals to ϕM_d, d is average diameter of the magnetic nanoparticles, k_B is the Boltzmann constant, H is magnitude of the magnetic field, T is the ferrofluid temperature.

Due to the negative sign in equation (4), diamagnetic particles tend to move toward regions where the magnetic field is weak. It is called negative magnetophoresis that depends on sizes.

Figure 2.4 shows the direction of the magnetic field. The size of the permanent magnet is much bigger than the size of the microchannel. Therefore we can estimate the magnetic force acting on the diamagnetic particle and the magnetic field are strictly in the y-direction [37]. Therefore the analytical expression for magnitude of 1D magnetic fields of a single rectangular permanent magnet of thickness T, width 2W and length 2L expresses as,

$$H(y) = \frac{M_s}{\pi}\left[tan^{-1}\left(\frac{(y+T)\sqrt{W^2+L^2+(y+T)^2}}{WL}\right) - tan^{-1}\left(\frac{y\sqrt{W^2+L^2+y^2}}{WL}\right)\right] \quad (6)$$

Where $M_s = 1.576 \times 10^5$ A/m is the residual magnetization of permanent magnet as calculated from the residual magnetic flux density, B_s=0.198 T through $M_s = \frac{B_s}{\mu_0}$.

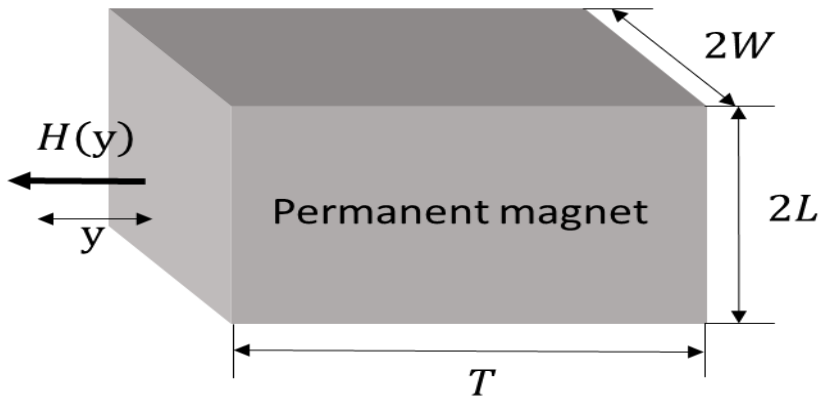

Figure 2.4. The 1D magnetic field for rectangular permanent magnet.

2.3. Hydrodynamic viscous drag force

Hydrodynamic viscous drag force is occurred by the velocity difference between particle and surrounding fluid. We take the Stokes' law for drag on a spherical particle in a low Reynolds number flow [38].

$$\mathbf{F}_{\mathrm{d}} = 3\pi\eta \mathrm{D}_{\mathrm{p}}(\mathbf{v}_{\mathrm{f}} - \mathbf{v}_{\mathrm{p}})\mathrm{f}_{\mathrm{D}} \tag{7}$$

Where η is viscosity of the fluid, $\mathrm{D_p}$ is diameter of spherical diamagnetic particle, $\mathbf{v}_{\mathrm{f}}$ is a velocity vector of the fluid, $\mathbf{v}_{\mathrm{p}}$ is a velocity vector of the particle, and $\mathrm{f_D}$ is hydrodynamic viscous drag coefficient. Its expression takes the form of

$$f_D = \left[1 - \frac{9}{8}\left(\frac{a_p}{\delta}\right) + \frac{1}{2}\left(\frac{a_p}{\delta}\right)^3\right]^{-1} \tag{8}$$

Where a_p is radius of the spherical diamagnetic particle, and δ is the distance from the diamagnetic particle center to the microchannel wall [13, 39].

In order to develop hydrodynamic viscous drag force, we need to define the axial flow velocity. We assume fully developed laminar channel flow with the velocity profile parallel to x-direction. Thus, the expression for x-direction fluid velocity is given by

$$v_{fx} = \frac{3Q}{8w_c h_c}\left[1 - \left(\frac{y}{w_c}\right)^2\right] \tag{9}$$

In which Q is volumetric flow rate, and $\mathrm{w_c}, \mathrm{h_c}$ are the width and height of the microchannel, respectively.

2.4. Particle velocity

This diamagnetic particle in paramagnetic fluid system under external magnetic fields is governed by several force including magnetophoretic repulsion force, viscous drag force, particle/fluid interactions, gravity, buoyancy force, thermal kinetics, and interparticle effects [35, 40]. It has be shown that aforementioned forces are negligible instead of magnetophoretic repulsion force and viscous drag force. Therefore we only consider about two dominant forces. Given these forces, we developed the equation of motion for a diamagnetic particle in the microchannel, based on a Lagrangian particle tracking method and Newton's law.

$$m_p \frac{dv_p}{dt} = \mathbf{F}_m + \mathbf{F}_d \tag{10}$$

Where m_p, v_p are the mass and velocity of the diamagnetic particle, and $\mathbf{F}_m$, $\mathbf{F}_d$ are the magnetophoretic repulsion acting on the particle and hydrodynamic drag forces, respectively.

The size of the permanent magnet is much bigger than the size of the microchannel. Thus, the rectangular magnet placed parallel to the microchannel assumes that the magnetophoretic repulsion force is only acting on the positive y-direction [37]. In other words, we neglect the contribution of magnetophoresis the x-direction. Equation of motion of particle as follows

$$m_p \frac{dv_{py}}{dt} = F_{my} + F_{dy} \tag{11}$$

In which m_p and, v_p are the mass and velocity of the diamagnetic particle, and F_{my} and F_{dy} are the magnetophoretic repulsion acting on the particle and hydrodynamic drag forces in y direction, respectively. F_{my} is defined as

$$F_{my} = -\frac{2\pi\mu_0\phi {a_p}^3 M_d L(\alpha)\nabla H^2}{3H} \quad (12)$$

We assume the expanding channel as rectangular channel that the streamline is only parallel to the magnet. Therefore v_{fy} is negligible in y-direction. Thus, F_{dy} is reduced as

$$F_{dy} = -3\pi\eta D_p v_{py} f_D \quad (13)$$

Substituting the parameters, we obtain the particle velocity in a y-direction, v_{py}, as

$$v_{py} = -\frac{\mu_0\phi {a_p}^2 M_d L(\alpha)\nabla H^2}{9\eta f_D H}\left(1 - e^{-\frac{6\pi a\eta f_D}{m_p}t}\right) \quad (14)$$

Therefore, diamagnetic microparticles deflection increase with increasing of the ferrofluid nanoparticles concentration, ϕ, radius of diamagnetic particle , a_p, Langevin function, $L(\alpha)$, fluid viscosity, η, and drag coeffieient, f_D.

2.5. Calculation of particle trajectory

Based on the above analysis, we obtain 2D theoretical trajectories of diamagnetic particles in paramagnetic solution in response to magnetic field gradients. The instantaneous x-position of the particle, r_{px}, and instantaneous y-position of the particle, r_{py}, are obtained by integrating the particle velocity over time.

$$r_{px} = r_{0x} + \int_0^t v_{fx}(t')dt' \quad , \quad r_{py} = r_{0y} + \int_0^t v_{py}(t')dt' \quad (15)$$

In which r_{0x} is the initial x-location of the particle, r_{0y} is the initial y-location

of the particle, and t is the time coordinate [13]. The particle/fluid interactions, gravity, thermal kinetics, and interparticle effects are neglected.

2.6. Elasto-inertial particle focusing

Particle migration under laminar flow conditions was first studied in early experiments of segré and Silberberg [41]. Recently many studies have been reported on inertial particle migration in channels with square cross section. The forces acting on particles suspended in fluids are the wall repulsion lift force and the shear gradient lift forces [6, 42].

The wall repulsion lift force, $F_{L,W}$, drives the particles away from the channel wall and moves the particles towards the channel centerline. The shear gradient lift force, $F_{L,S}$, pushes the particles away from the centerline. The equilibrium position of the particles is determined by force balancing, Reynolds number, and blockage ratio, defined as $\kappa = D_p/D_h$ with D_p is the particle diameter, D_h is the hydraulic channel diameter, [14]. Therefore the net lift force scales as [7]

$$F_L = f_L(Re, x_c)\frac{\rho U^2 {D_p}^4}{D_h^2} \tag{16}$$

Where $f_L(Re, x_c)$ is a lift coefficient that is a function of the channel Reynolds number and cross section of the channel. Therefore the net lift varies from the channel Reynolds number and cross section. D_p is the particle diameter, and D_h is the hydraulic channel diameter. Traditionally, in the micro-scale geometries, Reynolds number deduced as

$$Re = \frac{\rho U D_h}{\eta_0} = \frac{2\rho Q}{(w_c + h_c)\eta_0} \tag{17}$$

In which ρ is the fluid density, $U = Q/(w_c h_c)$ is the average flow velocity, Q is the volumetric flow rate, η_0 the zero-shear viscosity and the hydraulic diameter is given by $D_h = 2w_c h_c/(w_c + h_c)$, and w_c , h_c are the width and the height of the microchannel, respectively [43].

Non-Newtonian fluids provide another mechanism for particle migration under the laminar flow conditions. Mason and coworkers [44] observed different particle migration phenomenon depending on the polymeric fluids properties. Under the viscoelastic fluids, particles move towards the channel centerline and they are affected by additional force, such as the elastic force, F_e. The elastic force is contribute to the particle migration effecting on the first normal stress difference$(N_1 = \sigma_{xx} - \sigma_{yy})$. The second normal stress difference $(N_2 = \sigma_{yy} - \sigma_{zz})$ is negligible in our experiments [23]. The elastic force exerts on the particle scales as

$$\mathbf{F}_e = A{D_p}^3 \nabla N_1 \tag{18}$$

In which A is empirical constant [32, 45].

Using upper convected Maxwell model we developed the first normal stress difference, $\mathbf{N_1} = 2\mu\lambda\dot{\boldsymbol{\gamma}}^2$ [14]. The elasticity is characterized by the dimensionless quantities: Weissenberg number, Wi . In the microchannel system, the Weissenberg number is defined by

$$Wi = \lambda\dot{\gamma}_c = \frac{\lambda U}{w_c/2} = \frac{\lambda Q}{h w_c^2/2} \tag{19}$$

In which λ is the relaxation time, $\dot{\gamma}_c$ is the average shear rate defined at the average velocity U.

For viscoelastic fluid, two dimensionless quantities (Wi,Re) compete each

other and make the particle alignment at the centerline of the channel (figure 2.5). Elasticity number is defined as the ratio of the Weissenberg number to the Reynolds number by introducing a dimensionless number to evaluate the relationship between inertia to elasticity.

$$El = \frac{Wi}{Re} = \frac{\lambda \eta_0 (w_c + h_c)}{\rho w_c^2 h_c} \tag{20}$$

The preconditions for particle focusing is as follows: when the ratio of the particle size to channel dimension is not less than ~0.1 [23].

(a)

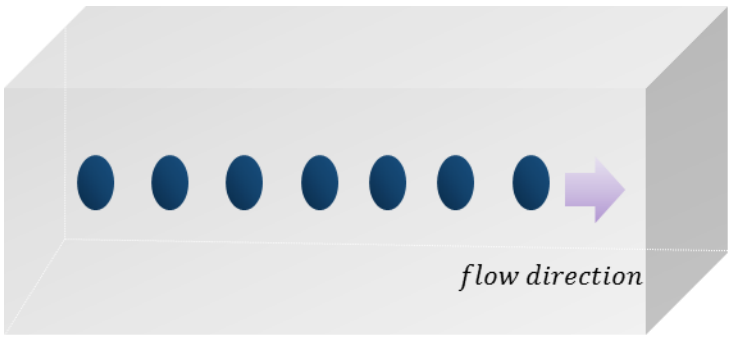

(b)

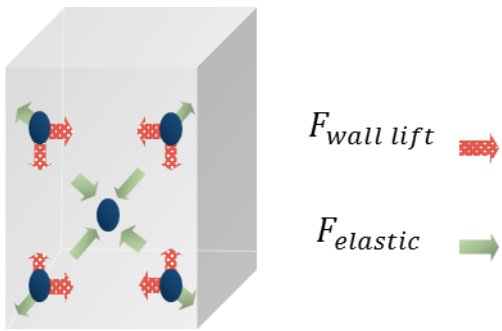

Figure 2.5. Schematic illustration of (a) the particle alignment: "elasto-inertial particle focusing" (b) the force mechanism of viscoelastic flows.

III. EXPERIMENTS

3.1. Device fabrication

Figure 3.1 and 3.2 show pictures of microfluidic devices used in our experiments. Devices were fabricated by using standard soft lithography techniques. A polydimethylsiloxane (PDMS) (Sylgard 184, Dow Corning) were poured onto the SU-8 master at a 10:1 ratio of based to crosslinker, degassed in a vacuum chamber, and cured in an oven at 70℃ for 6 hours. The devices were then cut from the mold; ports are punched with a sharpened flat-tip needle and devices were bonded to glass slides through oxygen plasma treatment. After plasma treatment and placement onto the glass substrate the devices were maintained at 80 ℃ in a furnace for 20 min to increase bonding. Dimensions of the microfluidic channel are listed in figure 3.1 (b), 3.2 (b). One NdFeB permanent magnet was used to produce required magnetic fields for separation. Residual magnetic flux density of magnet, B, was measured to be 0.198 T by a Tesla meter(TM-701 KANETEC). Each magnet is 10 mm in thickness, 2 mm in length, and 5 mm in width. The magnet was embedded into the PDMS slab with the direction normal to the microchannel or the flow direction in our experiment. It were positioned 500μm away from the microchannel [46].

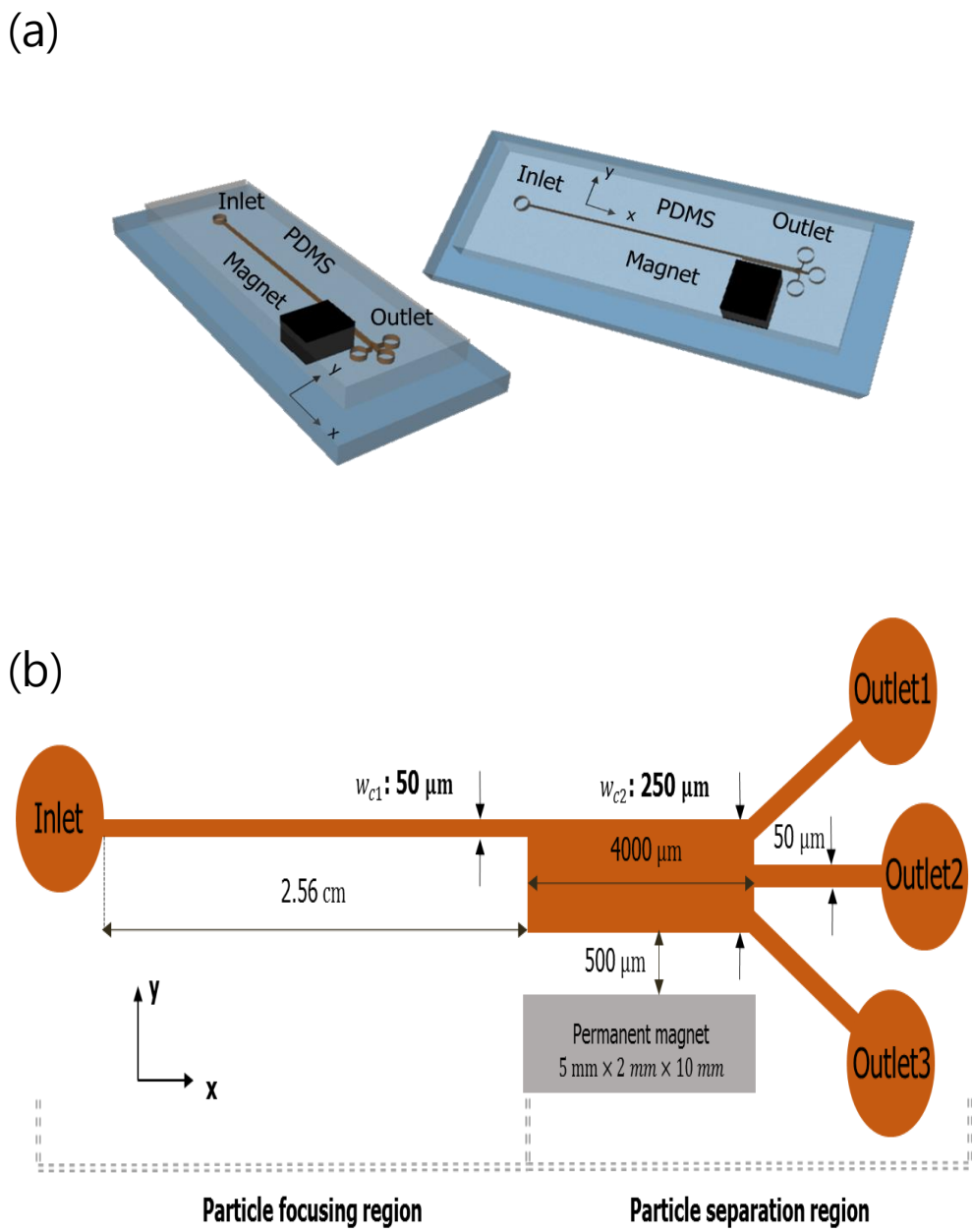

Figure 3.1. (a) A schematic representation of the microchannel device for particle separation with a permanent magnet. (b) *Topview* of the system and the dimensions of the microfluidic channel.

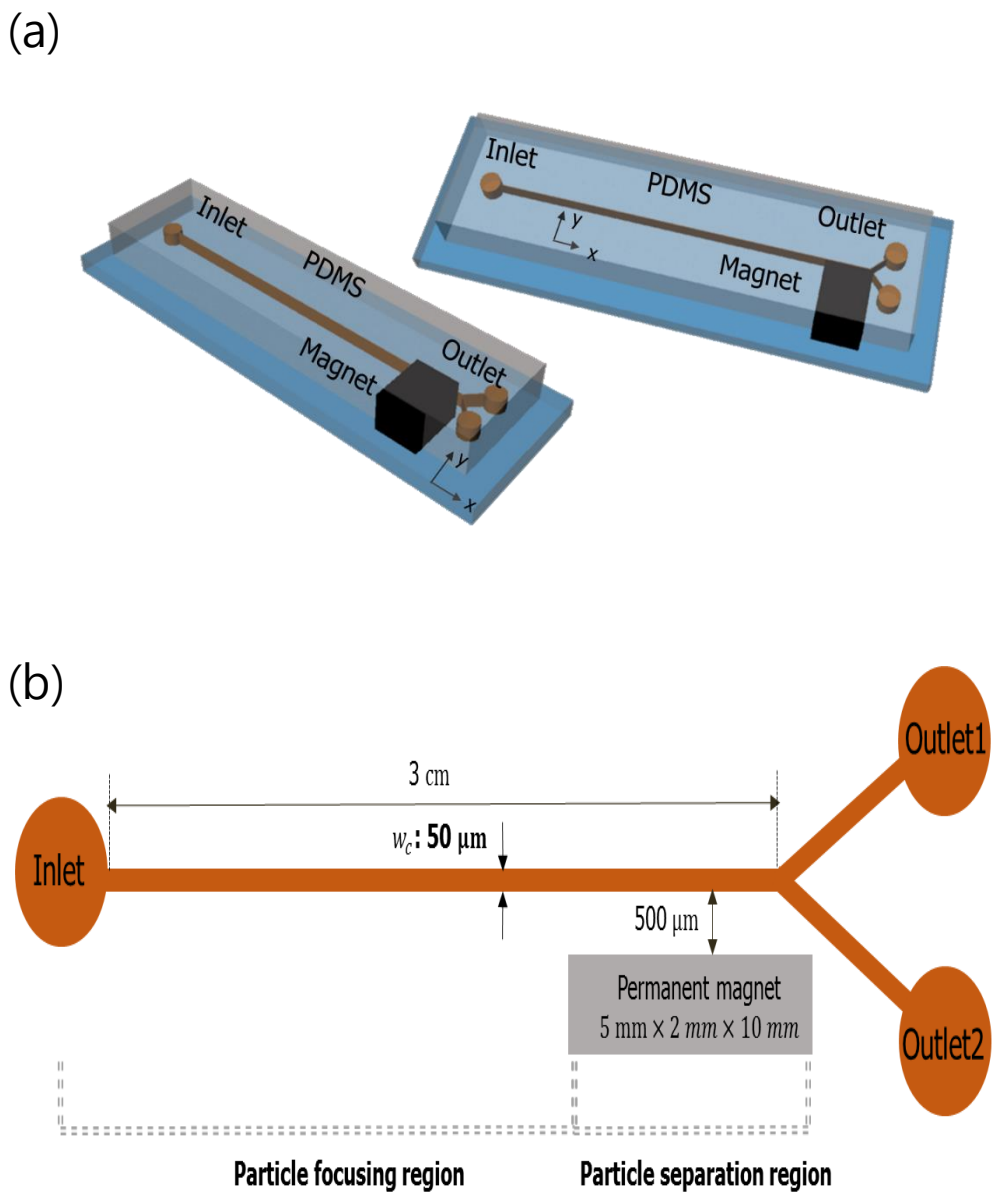

Figure 3.2. (a) A schematic representation of the microchannel device to find the suitable conditions for particle separation with a permanent magnet. (b) *Topview* of the system and the dimensions of the microfluidic channel.

3.2. Preparation of particle suspensions

To show the evidence of size-based separation, two types of polystyrene particle (intrinsically a diamagnetic particle [47]) were used in these experiments. 5 μm-diameter diamagnetic polystyrene particles (Bangs Labortories, Inc.) and 20 μm-diameter diamagnetic polystyrene particles (Polyscience, Inc.) were mixed and re-suspended in two types of media [48]; Newtonian media and viscoelastic media.

For Newtonian media, the DI water-glycerol solution was prepared at a volume ratio of 7.8:2.2 in order to match the density of polystyrene particles ($1.05\mathrm{g}/m^3$) (figure 3.3) [20]. As a viscoelastic media, PEO (poly (ethyleneoxide), $M_w = 1{,}000{,}000$, Sigma Aldrich) was added to DI water in 0.05, 0.1, 0.2, 0.3, 0.4, 0.5, 0.6, and 0.7 wt % , respectively. Then the DI water-PEO solution was prepared at a volume ratio of 7.8:2.2 in order to match the density of polystyrene particles ($1.05\mathrm{g}/m^3$) (figure 3.4).

A water based ferrofluid, EMG 408 (Ferrotec Corp.) contains 1.2% magnetic nanoparticles (10 nm diameters) in volume and has a saturation magnetization of 5252 A/m (corresponding to 6.6 mT as per manufacturer) [49]. The EMG408 was diluted with two types of media to 0.01, 0.03, 0.05, 0.07, 0.1, 0.125, 0.15, and 0.175 × its original concentration, respectively. A small amount of surfactant (Tween 20 (0.01wt %) (Sigma Aldrich)) was added to prevent particle aggregation in the suspension. The mixture was sonicated for 20 min to prevent aggregation each other (figure 3.3 and 3.4).

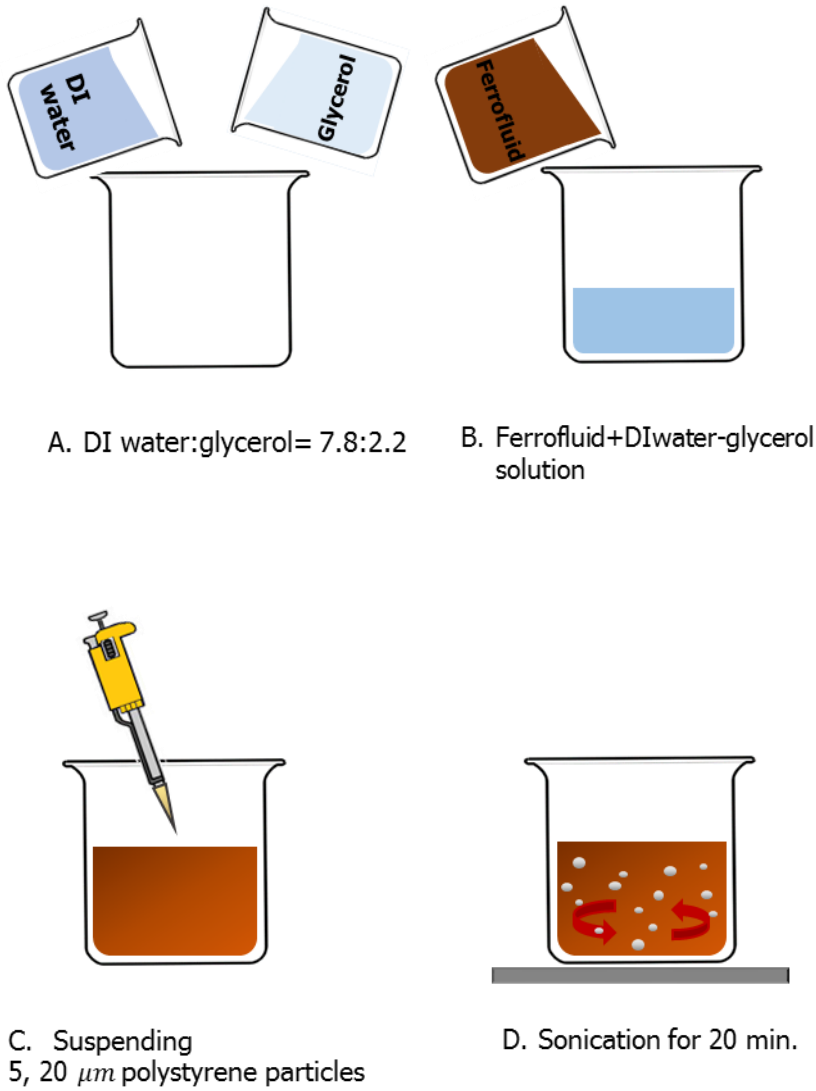

Figure 3.3. A schematic representation of preparing process of Newtonian suspension.

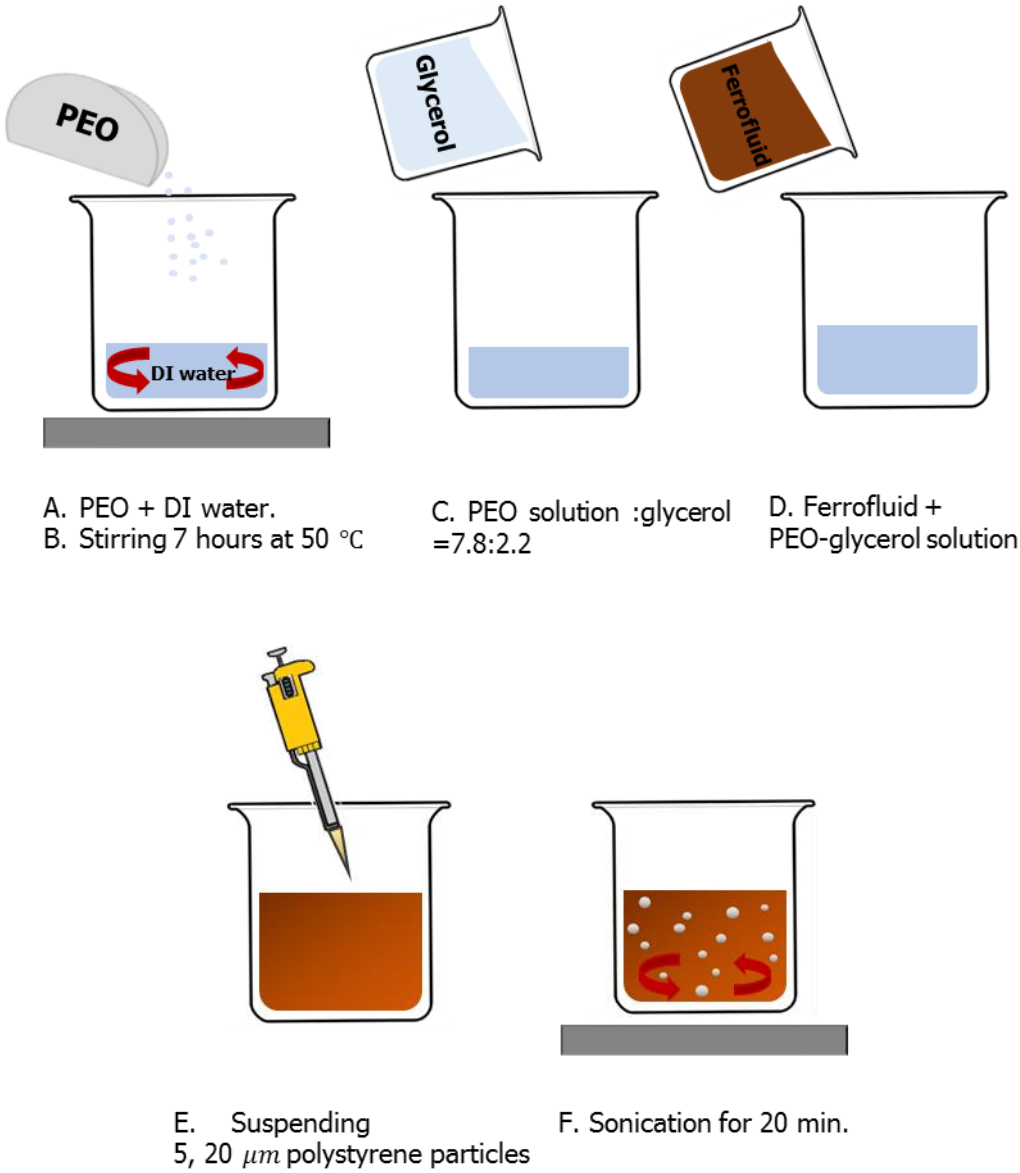

Figure 3.4. A schematic representation of preparing process of viscoelastic suspension.

3.3. Particle manipulation and visualization

The particles in PEO / ferrofluid solution were driven through the channel by a syringe pump (KDS-200, KD Scientific). Tygon tubing was used to connect to the syringe pump to the channel and to deliver the solution into the channel. Particle motion was visualized and recorded using inverted microscope (IX53, Olympus). The obtained images were processed using Image-Pro Plus 6.0 software (Media Cybernetics, Silver Spring, USA).

3.4. Measurement of rheological properties

A measurement of rheological properties of PEO / ferrofluid solution is important to understand this experiment. In this experiment, the magnetoviscous effect is negligible. Therefore the viscosity of fluids were measured using a controlled shear stress rheometer (AR G2, TA Instruments) with 60 mm parallel plate cell at shear rates of $0.5 < \dot{\gamma} < 10^{-3}s^{-1}$. Due to their low viscosity, it is hard to get the reliable storage modulus data. Therefore, the relaxation time of the PEO / ferrofluid solution was measured by the capillary break up extensional rheometer (CaBER, ThermoHaake) [50]. The relaxation time was obtained by the equation (21). The filament radius is found to decrease exponentially with time and showed an inverse relationship with the relaxation time of the solution, according to

$$R_{min} = \left(\frac{GR_0^4}{\sigma}\right)^{1/3} \exp\left(\frac{-t}{3\lambda}\right) \quad (21)$$

Where λ is the characteristic relaxation time of the fluid, G, is the elastic modulus, R_0, is the filament radius after the separation of the end-plates in the capillary break up experiments [51].

VI. RESULTS AND DISCUSSION

4.1. Rheological properties of the PEO / ferrofluid solution

4.1.1. Shear thinning behavior

The obtained data of viscosity versus shear rate is given in figure 4.1 and figure 4.2. Figures show that the viscosity of PEO / ferrofluid solution is decreased as shear rate increased, showing shear-thinning behavior. This behavior can be explained by the assumption that nanoparticles in the suspension break their clustering chains and arrange their molecular under high shear rate [52, 53].

The viscosity increases as the weight fractions of PEO and ferrofluid respectively, increasing in the solution (as seen in figure 4.1, 4.2). Since the viscosity of ferrofluid increase without magnetic fields depends on two parameters: total volume fraction of magnetic nanoparticles,ϕ, and average diameter of nanoparticles,d. Therefore, increasing of the weight fractions of ferrofluid rises viscosity of the solution [25, 54].

Using proper viscosity model such as Cross model and Carreau model, we can estimate zero shear viscosity and infinite viscosity of solution, respectively.

$$\text{Cross model } \frac{\eta-\eta_\infty}{\eta_0-\eta_\infty} = \frac{1}{(1+(\lambda\dot{\gamma})^m)} \tag{22}$$

$$\text{Carreau model } \frac{\eta-\eta_\infty}{\eta_0-\eta_\infty} = \frac{1}{(1+(\lambda\dot{\gamma})^2)^{n/2}} \tag{23}$$

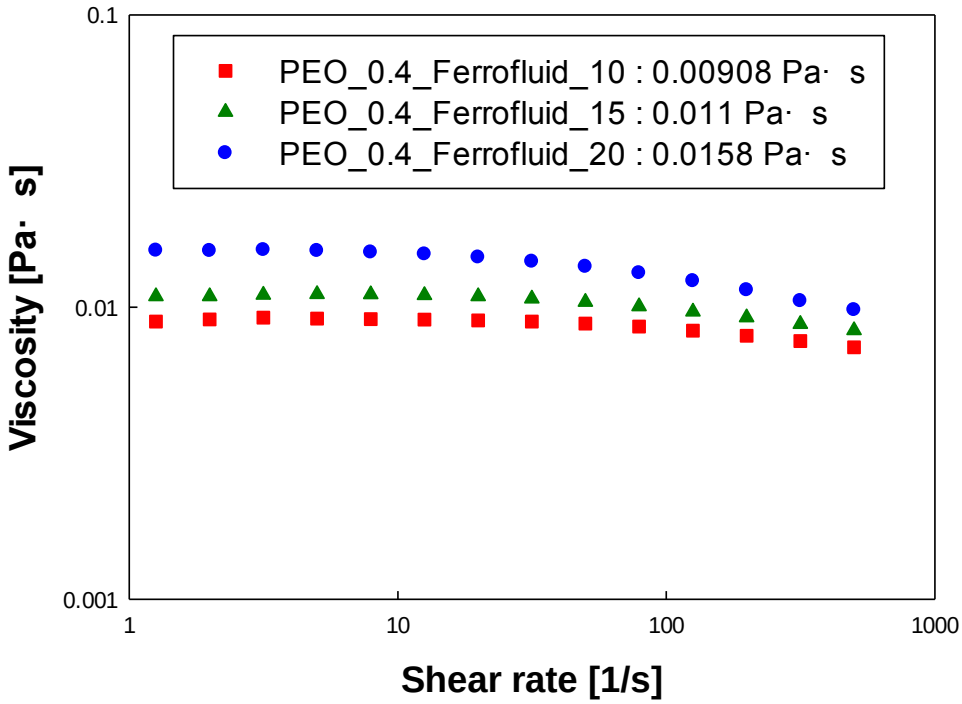

Figure 4.1. Viscosity versus shear rate according to the different ferrofluid concentration in the solution.

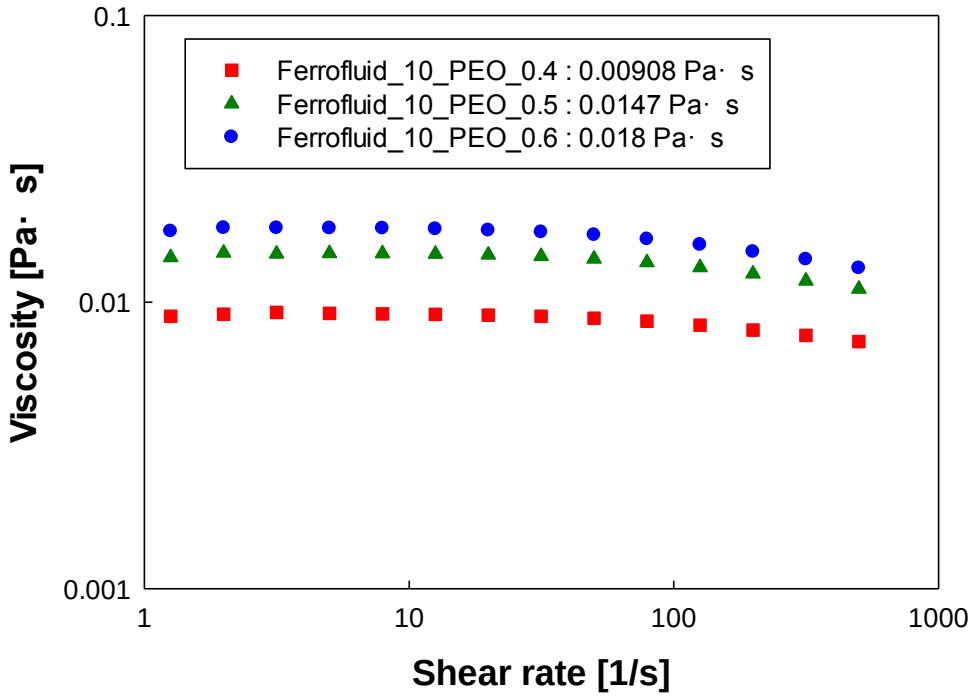

Figure 4.2. Viscosity versus shear rate according to the different PEO concentration in solution.

4.1.2. Dynamic viscosity

The solution in the microchannel experienced shear condition due to the channel wall. Therefore, to precise the viscosity of the solution, we need to consider the average shear rate acting on the channel. In micro-scale geometry, the average shear rate can be described as

$$\dot{\gamma}_c = \frac{U_{avg}}{h_c w_c^2/2} \tag{24}$$

In which $U_{avg} = Q/(w_c h_c)$ is the average flow velocity, and w_c, h_c are the width and the height of the microchannel, respectively. Substituting the experimentally results to the equation (22), (23), we obtained the dynamic viscosity of the solution. The dynamic viscosity of these solutions is provided in table4.1 for the different fluid conditions.

Table 4.1. Lists of rheological properties of solution used in experiments.

Sample	Relaxation time, λ	Zero shear viscosity, η_0	Dynamic viscosity, η
PEO 0.4wt% +FERROFLUID 10wt%	0.006340245	9.08E-03	9.08E-03
PEO 0.4wt% +FERROFLUID 15wt%	0.009135724	1.10E-02	1.10E-02
PEO 0.4wt% +FERROFLUID 20wt%	0.011265029	1.58E-02	1.57E-02
PEO 0.5wt% +FERROFLUID 10wt%	0.008907226	1.47E-02	1.46E-02
PEO 0.5wt% +FERROFLUID 12.5wt%	0.009457767	1.52E-02	1.52E-02
PEO 0.5wt% +FERROFLUID 15wt%	0.011596986	1.81E-02	1.80E-02
PEO 0.5wt% +FERROFLUID 20wt%	0.013427271	0.02286	2.23E-02
PEO 0.6wt% +FERROFLUID 10wt%	0.010344193	0.018	1.80E-02
PEO 0.6wt% +FERROFLUID 15wt%	0.013790517	0.02344	2.32E-02
PEO 0.6wt% +FERROFLUID 20wt%	0.016421332	0.02737	2.70E-02
PEO 0.7wt% +FERROFLUID 1.5wt%	0.014922255	0.02907	2.89E-02

4.1.3. Elasticity number

Elasticity number is defined as the ratio of the Weissenberg number to the Reynolds number.

$$\mathrm{El} = \frac{\mathrm{Wi}}{\mathrm{Re}} = \frac{\lambda \eta_0 (w_c + h_c)}{\rho w_c^2 h_c} \tag{20}$$

In which λ is the relaxation time, η_0 the zero-shear viscosity, ρ is the fluid density, and w_c , h_c are the width and the height of the microchannel, respectively.

The channel used in this experiment is shown in figure 3.1. Channel has two different channel width for the functionality; (1) particle focusing (w_{c1}: 50 μm), (2) particle separation (w_{c2}: 250 μm). Therefore the channel has two different elasticity number for one fluid condition. As seen in figure4.3, elasticity number is increased when the ratio of PEO in mixture increases. Also due to their channel size, elasticity number of particle separation area is relatively smaller than that of the particle focusing area. Therefore, the dominant force at the particle focusing area is elastic force and we excluded elastic force at the particle separation area. Thus, the dominant forces are magnetophoretic repulsion force and viscous drag force at the particle separation area (figure 4.4).

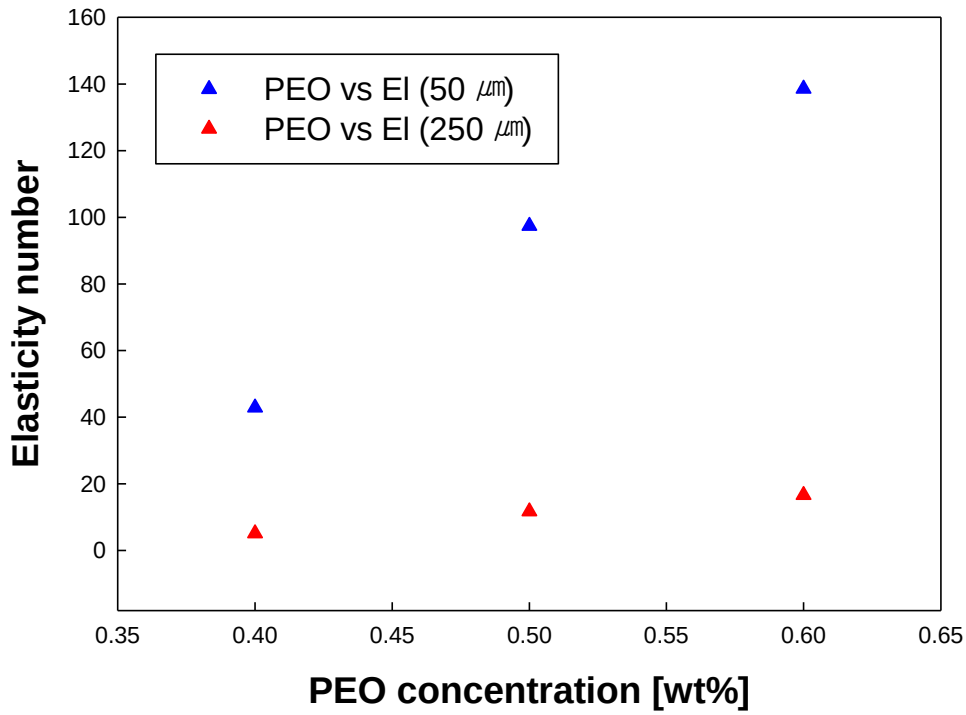

Figure 4.3. Elasticity number versus PEO concentration. Blue triangle demonstrates for particle focusing region (w_{c1}: 50 μm). Red triangle represents for particle separation region (w_{c2}: 250 μm).

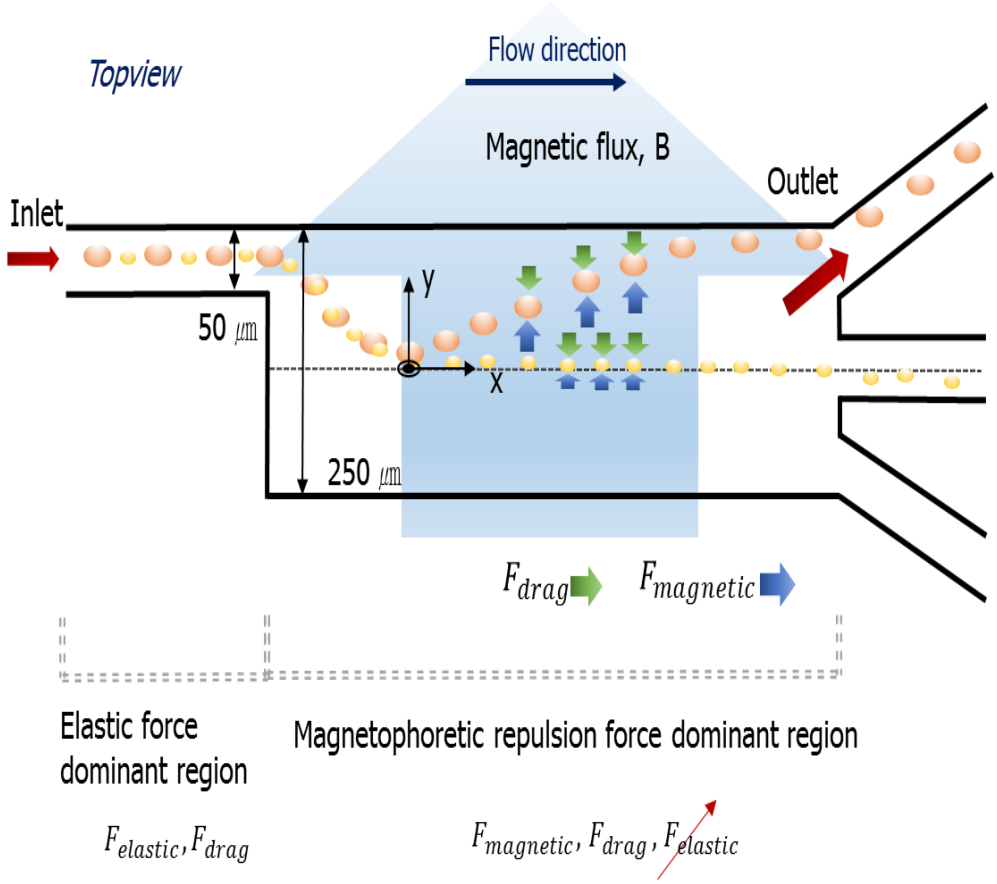

Figure 4.4. Schematic illustrating of the particle separation and force distribution.

4.2. Systematic study of particle separation

4.2.1. Decision of the proper conditions for diamagnetic particle separation

To verify the need of using the viscoelastic media for particle separation in microchannel system, we firstly used Newtonian media for the experiment. Figure shows distributions of $5, 20\mu m$ polystyrene particles that were recorded at four different axial position of the channel. Figure 4.5, 4.6 demonstrate the Newtonian fluid condition which contained DI water, glycerol and 0.1 × EMG408 ferrofluid flowing through the expanding channel at the volume flow rates of 50 $\mu l h^{-1}$.

Figure 4.5 shows the migration of the particles without an applied magnetic field condition. The diamagnetic particles flow randomly into the expanding channel (figure 4.5 (A), (B)) then flows randomly out toward the outlet (figure 4.5 (C), (D)). In this condition, the particles are not separate by size.

Figure 4.6 demonstrates the migration of the particles under the magnetic field. The diamagnetic particles flow randomly into the expanding channel (figure 4.6 (A), (B)). When the particles entered expanding channel, both types of particles experience negative magnetophoresis, therefore all particles repel away from the permanent magnet with their first position of the expanding channel (figure 4.6(C)). Thus size-based particle separation does not occur in this condition (figure 4.6 (D)).

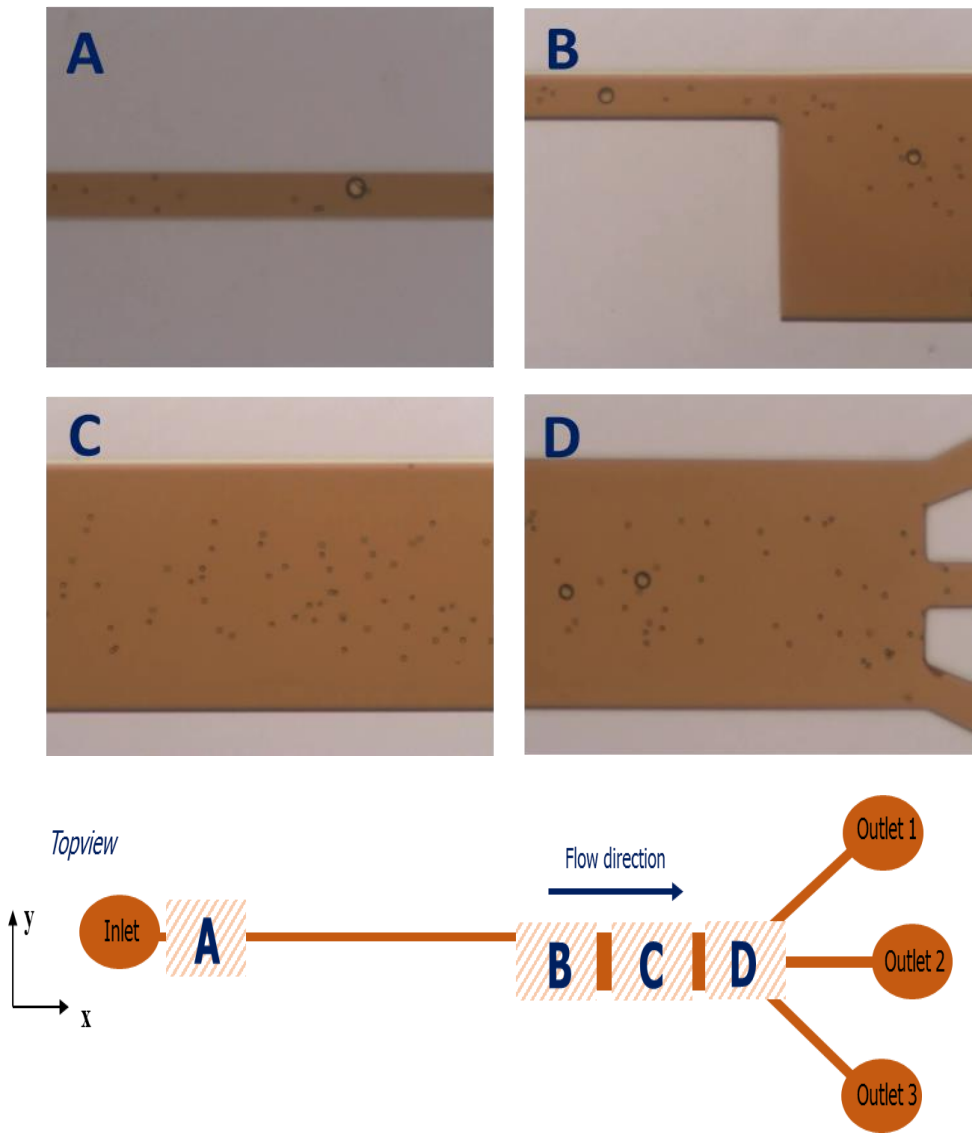

Figure 4.5. Migration of polystyrene particles in Newtonian fluid in the absence of the magnetic field. The image shows the distribution of 5 μm and 20μm diameter polystyrene particles at four different axial locations A-D.

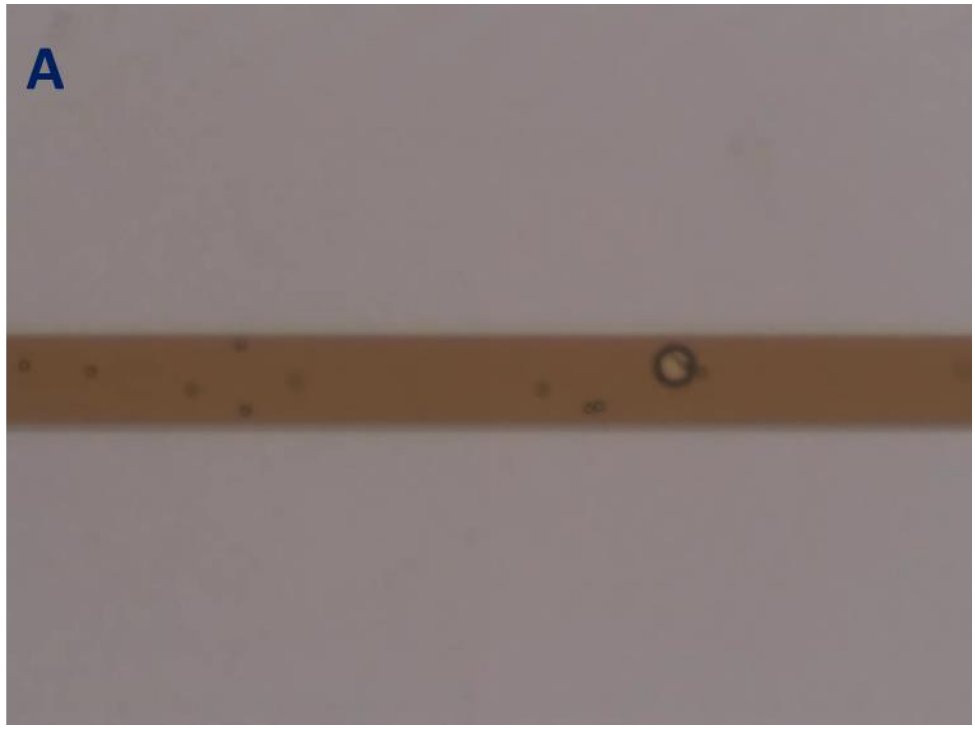
A

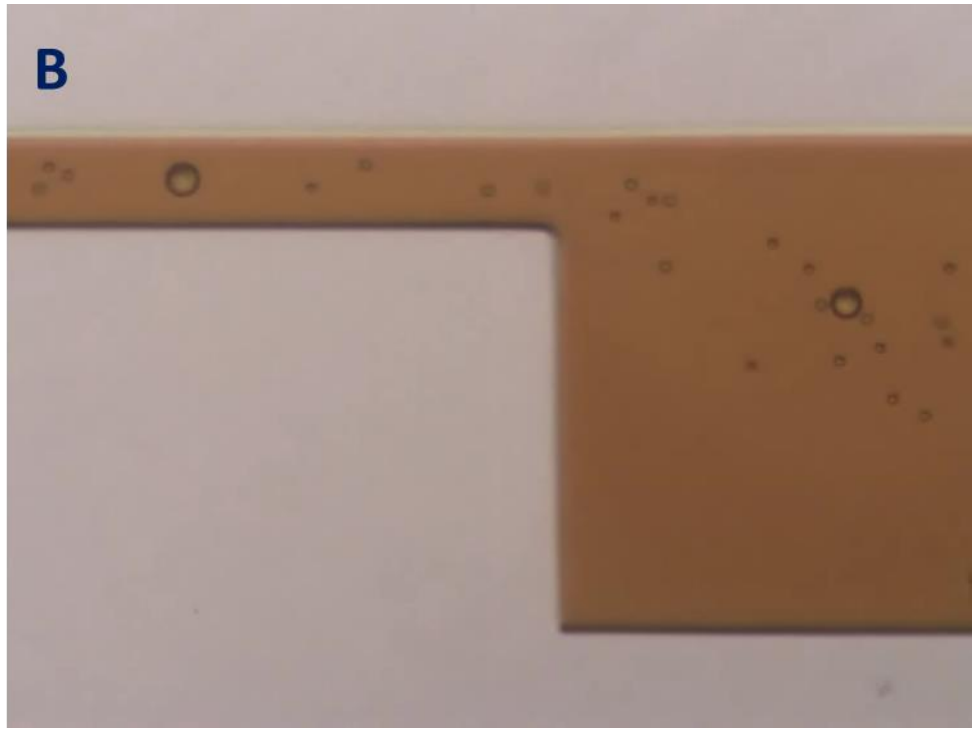
B


C

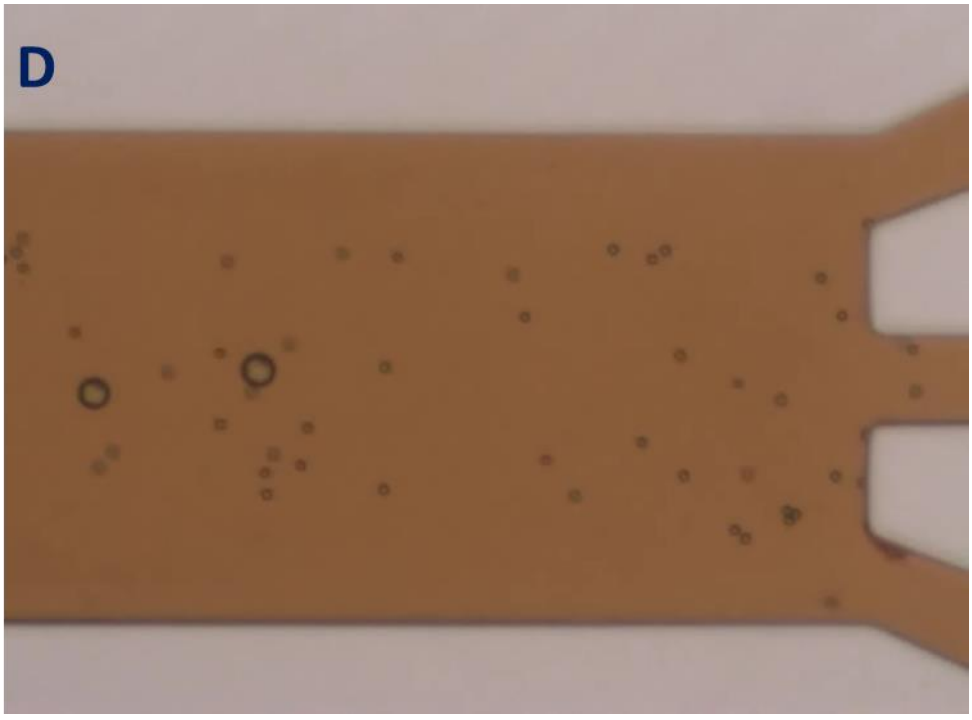
D

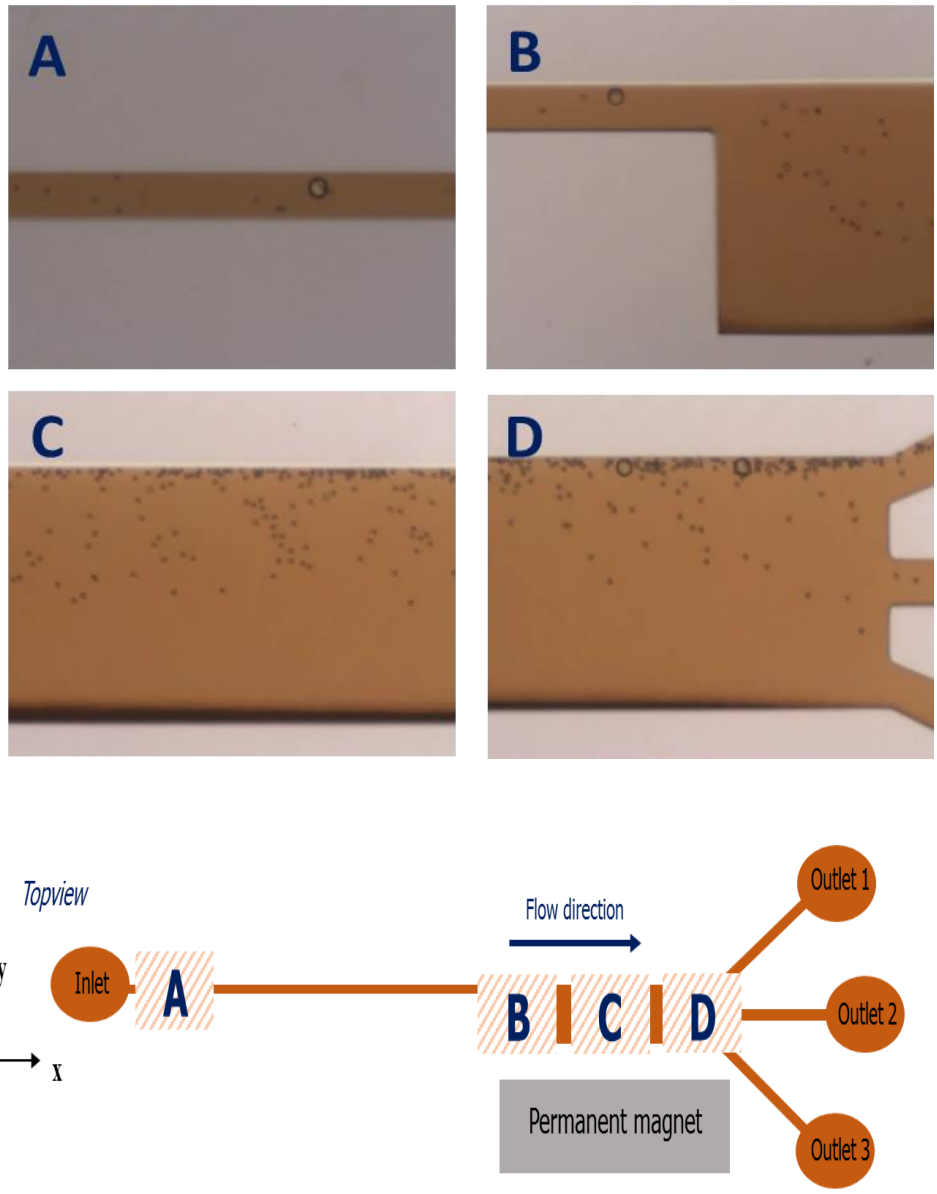

Figure 4.6. Migration of polystyrene particles in Newtonian fluid under the magnetic field. The image shows the distribution of 5 μm and 20 μm diameter polystyrene particles at four different axial locations A-D.

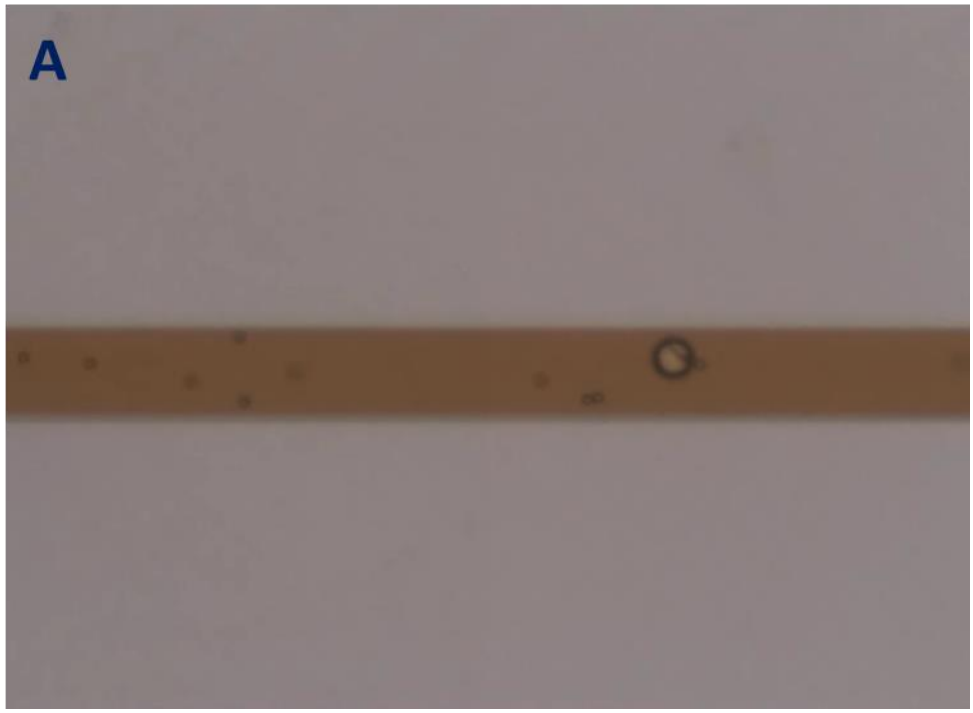
A


B

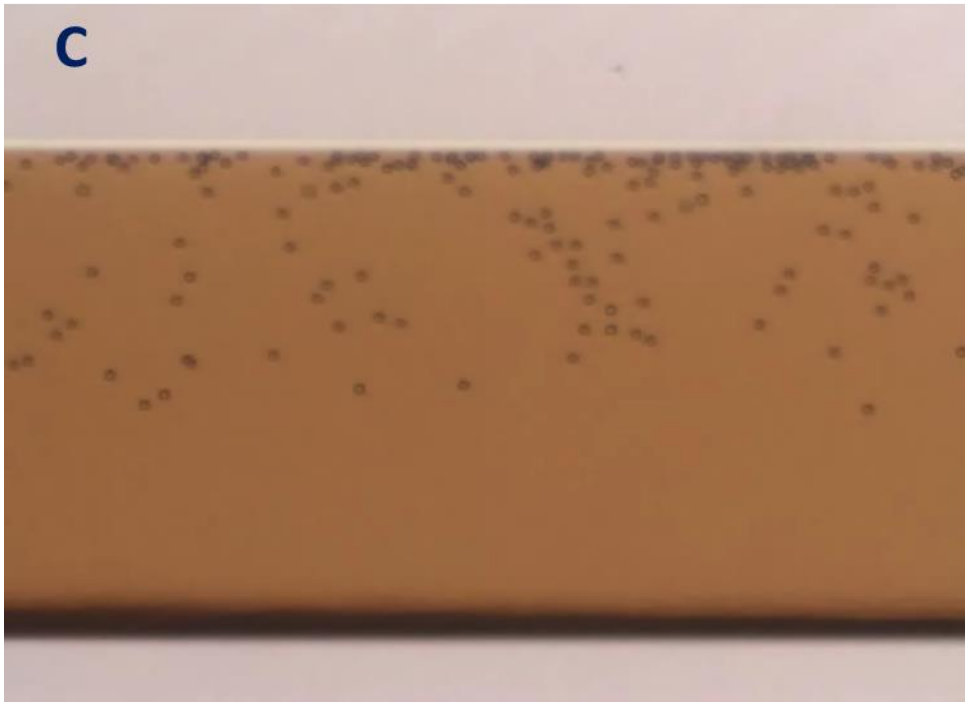
C

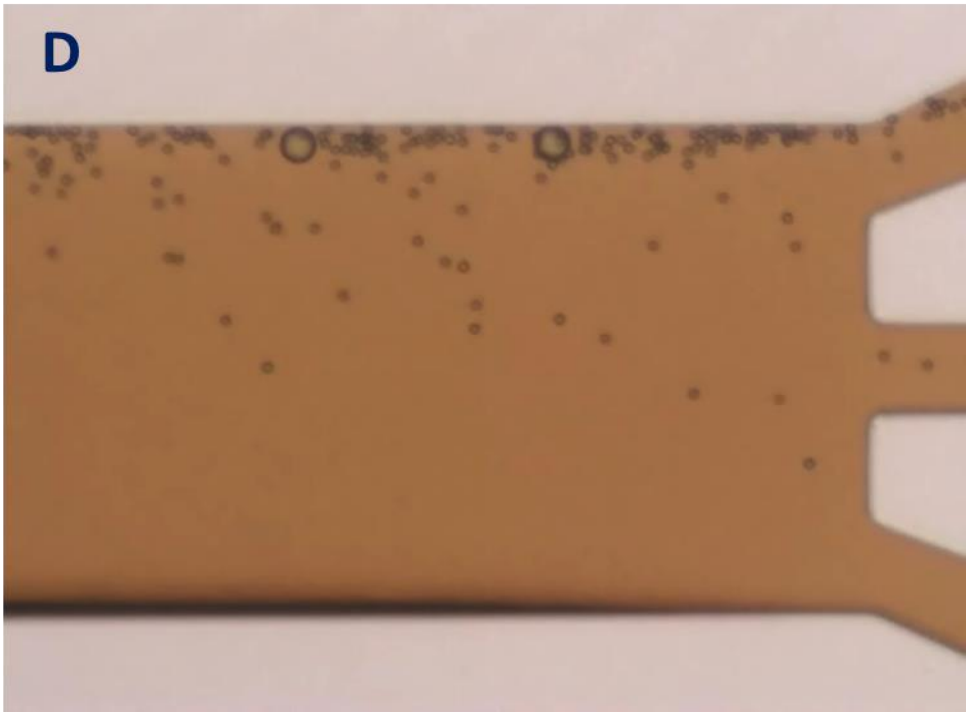
D

In viscoelastic fluid, there are lift force and elastic force. If the channel length is sufficiently long, the two forces compete each other and make the particle alignment in the centerline of the channel (w_{c1}: 50μm). This phenomenon is not occurred at the expanding channel (w_{c2} : 250 μm). Therefore negative magnetophoresis effectively occurs in this area. Thus, we expect synergistic effect of two phenomena for particle separation. To exert a synergistic effect on the micro-scale system, mixture ratio of the PEO and ferrofluid considered critical terms.

Thus, we make two constraints to find the experimental sets. First, PEO / ferrofluid solution has one equilibrium position in the microchannel. In other words, the particles focus in the centerline of the channel. Second, the formed particle alignment experience negative magnetophoresis and form newly alignment through lateral migration under the magnetic field. To satisfy the constraints, we conducted the experiment changing of the mixing ratio.

Using Y-shaped microchannel, we confirmed the experimental sets for particle separation in the expanding channel. Figure 4.7 shows the experimental results to find the proper condition for particle separation using Y-shaped microchannel. The conditions inside the square box satisfy the two constraints. Figure 4.9 shows one of the conditions corresponding to the square box in figure 4.8. We observed the particle focusing in the centerline due to the viscoselastic force without the magnetic field and the lateral migration due to negative magnetophoresis under the magnetic field (figure 4.9).

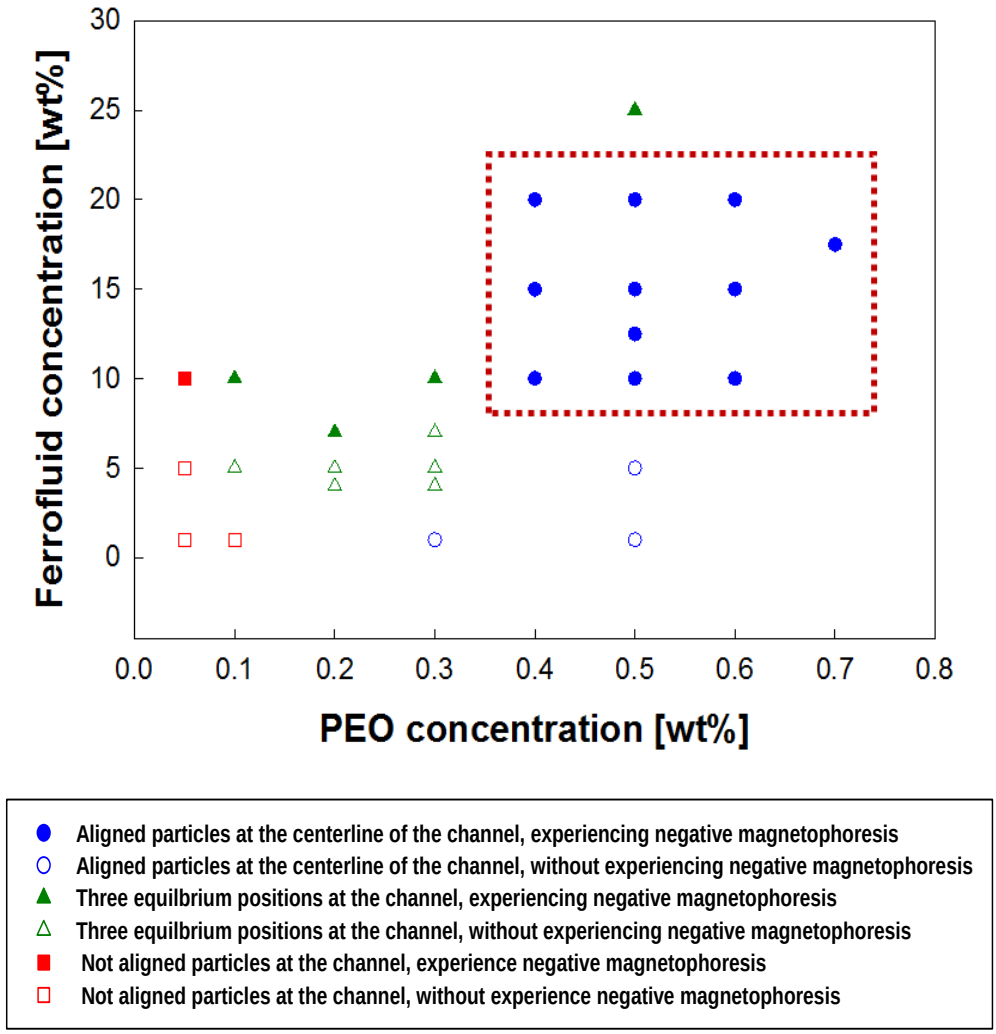

Figure 4.7. Experimental results to find the proper conditions for particle separation using Y-shaped microchannel. The conditions inside the square box satisfy the two constraints.

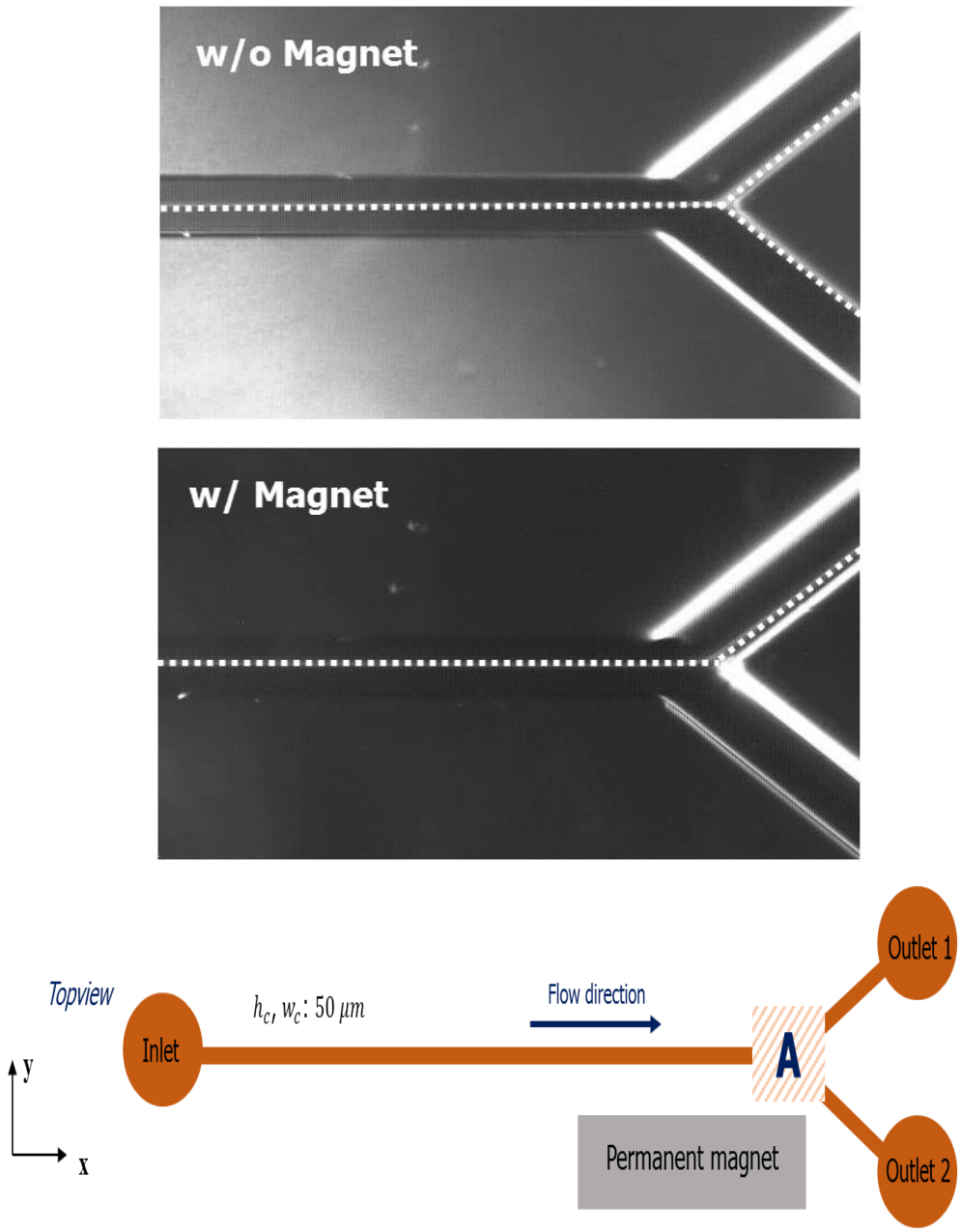

Figure 4.8. One of the conditions corresponding to the proper conditions (inside the square box in figure 4.7).

4.2.2. Size-based separation under the magnetic field : optimum conditions for particle separation

As shown in figure 4.9, 4.10, image shows distribution of 5 μm and 20 μm polystyrene particles at four different axial locations A-D.

The suspension consists of PEO 0.4 wt% in DI water mixed with glycerol solution containing ferrofluid 10 wt% at the volume flow rates of 50 $\mu l h^{-1}$. At the entrance of the channel, with a diameter of the 5, 20 μm diamagnetic particles randomly flow along each individual streamline (figure 4.9 (A)). The distance between channel inlet and expanding area is 2.6 cm that sufficiently long enough to particle focusing. Thus, two types of particles are focusing at the centerline of the channel until entered into the expanding area (figure 4.9 (B)). Elasticity number of the expanding area is relatively small enough than that of the focusing area. Thus, we excluded the elastic force in this expanding channel. Therefore without a magnetic field, the particles only flow by inertia in this section as shown in figure 4.9 (C). As a result, without a magnetic field condition, the particles move toward the outlet with their first position at the head of the expanding area (figure 4.9 (D)).

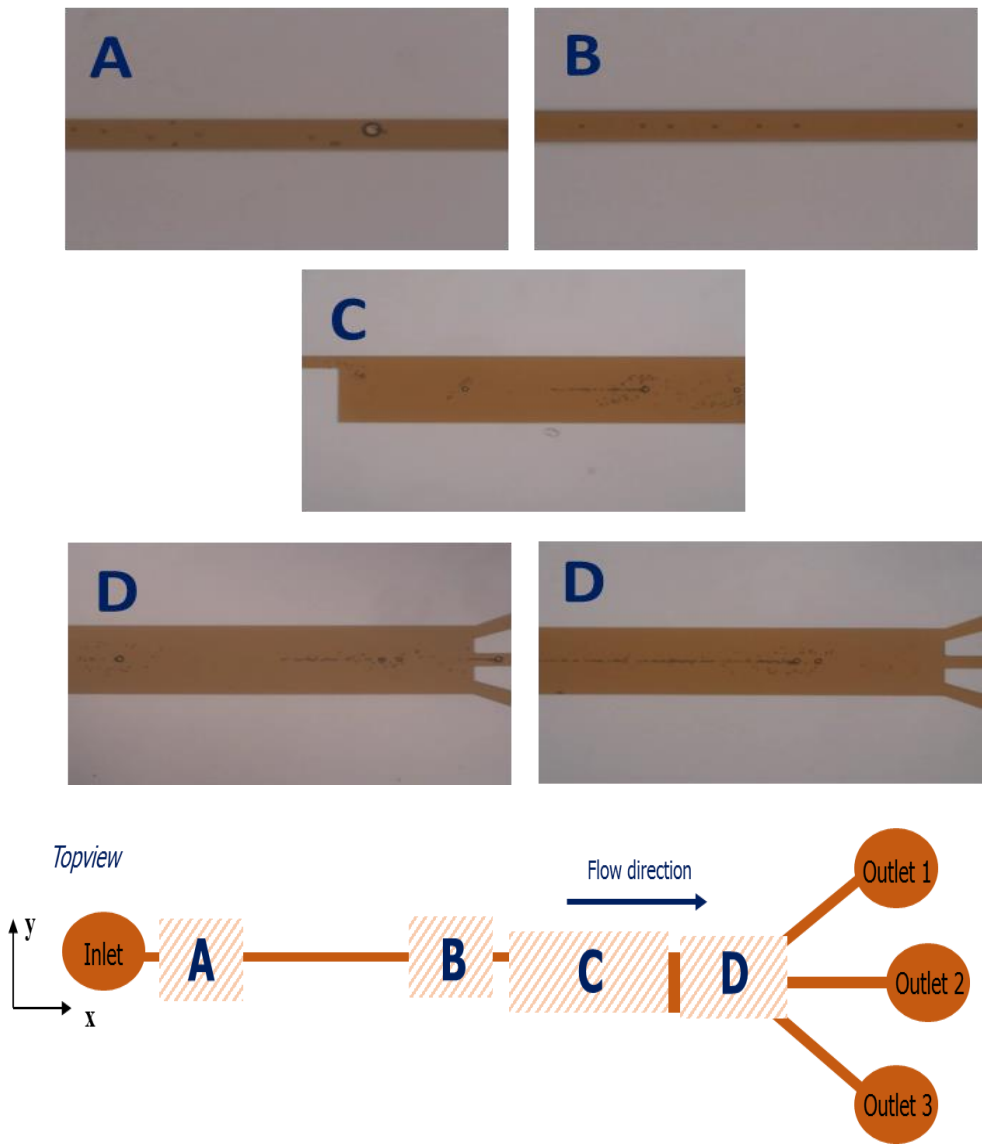

Figure 4.9. Migration of polystyrene particles in viscoelastic fluid (PEO 0.4 wt% in DI water mixed with glycerol solution containing ferrofluid 10 wt% at the volume flow rates of 50 µlh^{-1}) at the absence of the magnetic field. The image shows the distribution of 5 μm and 20μm diameter polystyrene particles at four different axial locations A-D.

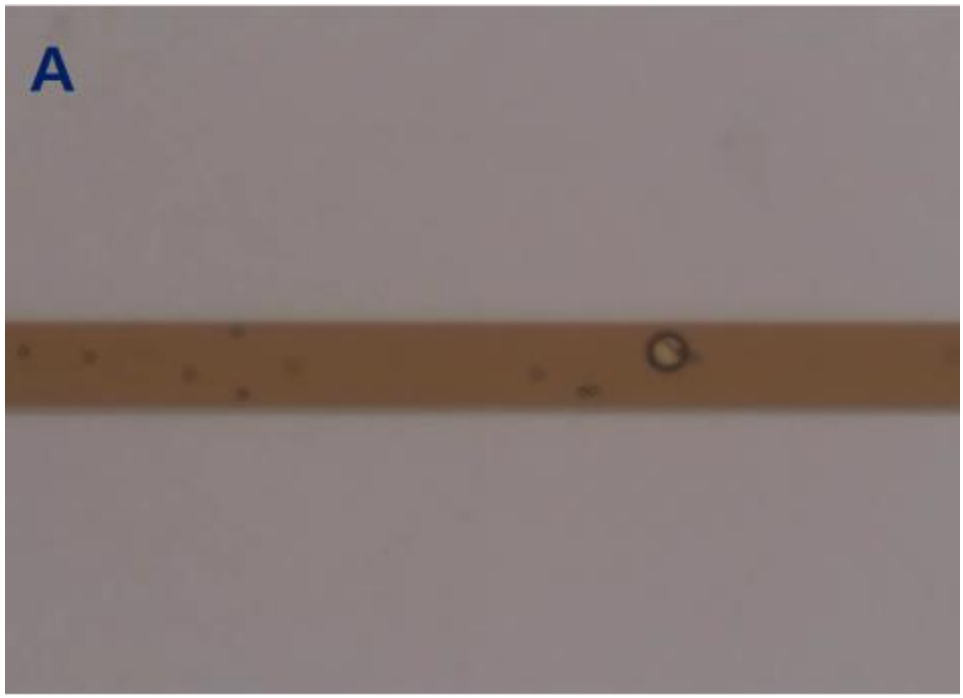
A

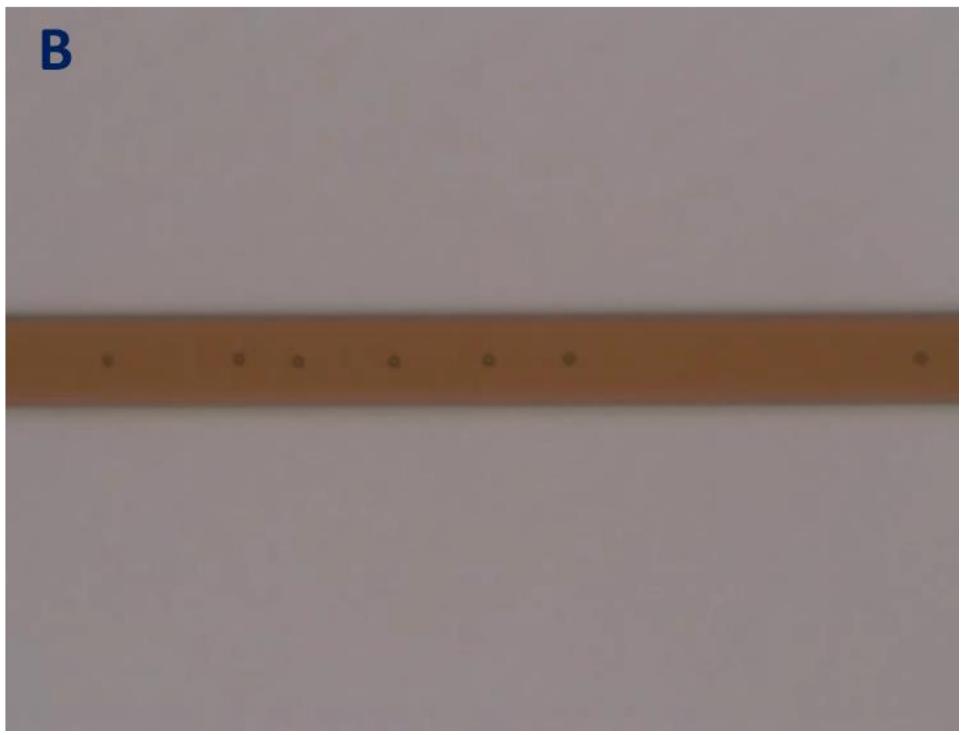
B

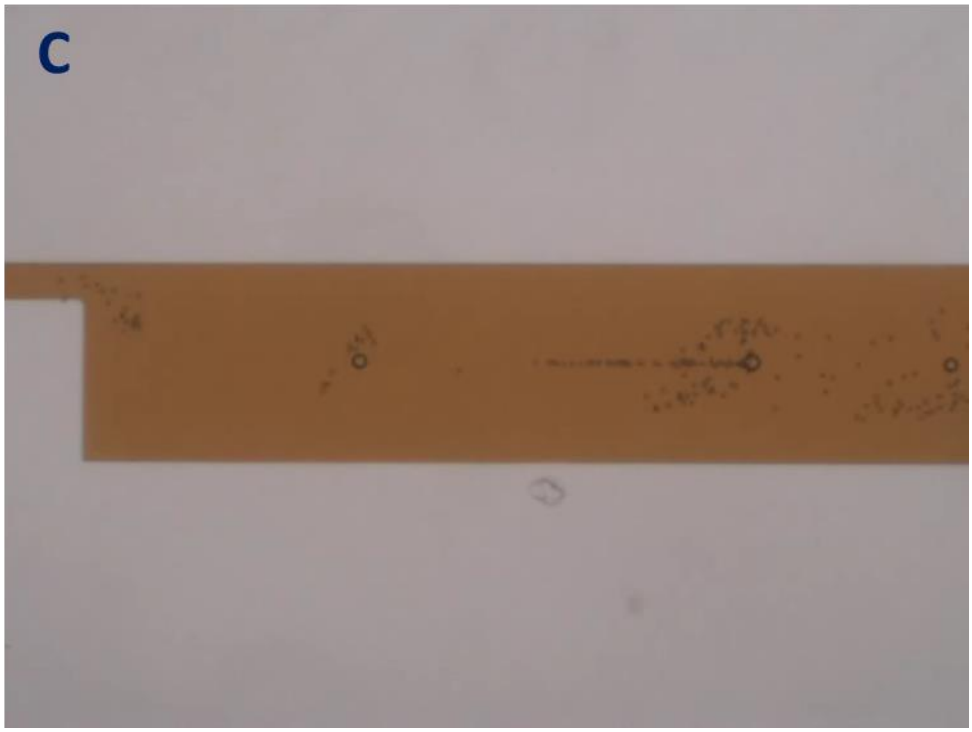
C


D

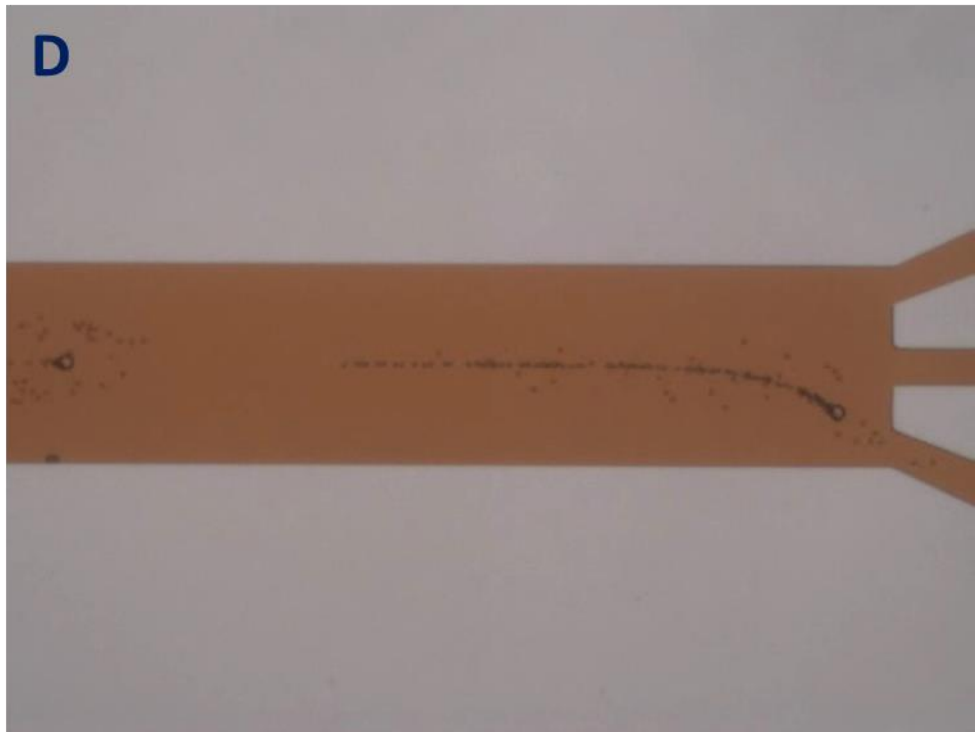
D

Under the magnetic field, the diamagnetic particles experience negative magnetophoresis. Figure 4.10 (A), (B) demonstrate that the particles (especially 20 μm particles) move toward regions where the magnetic field is weak. Therefore, diamagnetic particles get out of the flow direction and deflect along the positive y-direction [55]. Magnitude of the force acting on the particles is different from the particle size. Therefore larger size of the particle experience negative magnetophoresis more than smaller one (figure 4.10 (C)). As shown in figure 4.10 (D), with a diameter of 20 μm particles flowing along the side wall were collected through outlet1. 5 μm particles were collected through outlet2.

A graph of recovery rate is shown in figure 4.11. The recovery rate defines as the ratio of the total number of particles flew for 30 s to the number of the particles corresponding to each of the particle size flew for 30 s. 20 μm particles were collected at a 100% recovery rate through outlet 1. 5 μm particles were collected through outlet 3.

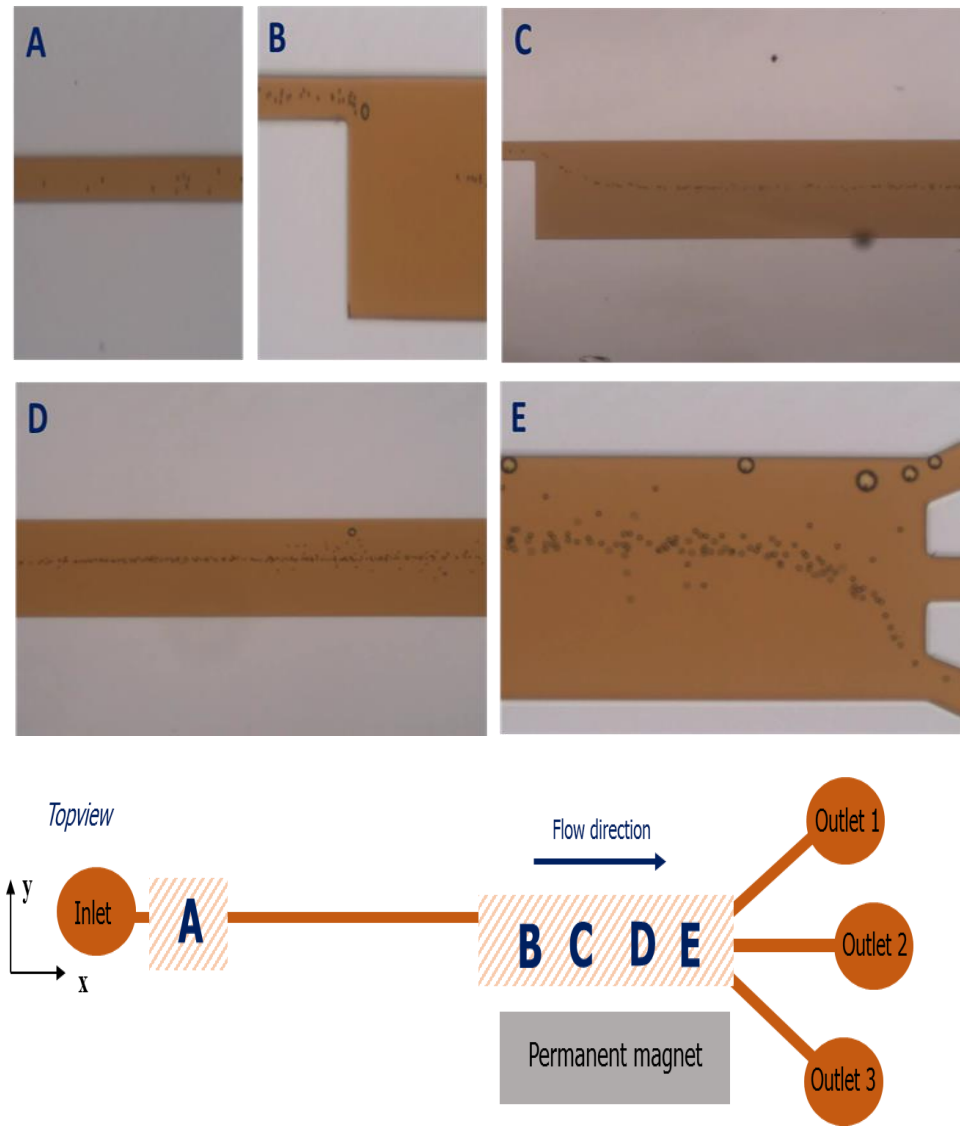

Figure 4.10. Migration of polystyrene particles in viscoelastic fluid (PEO 0.4 wt% in DI water mixed with glycerol solution containing ferrofluid 10wt% at the volume flow rates of 50 µlh^{-1}) under the magnetic field. The image shows the distribution of 5 μm and 20μm diameter polystyrene particles at five different axial locations A-E.

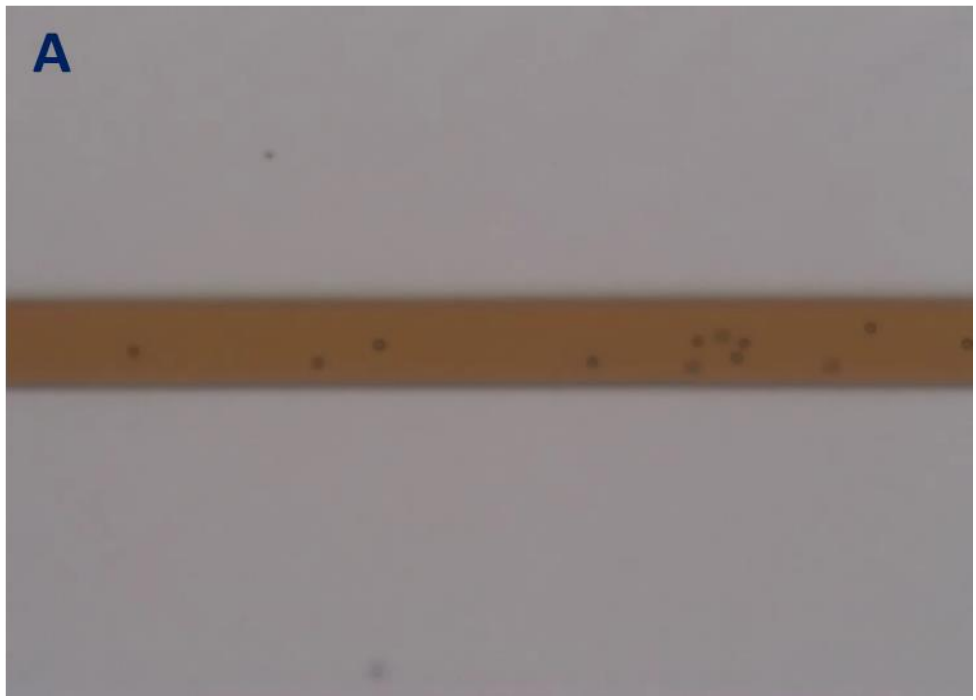
A

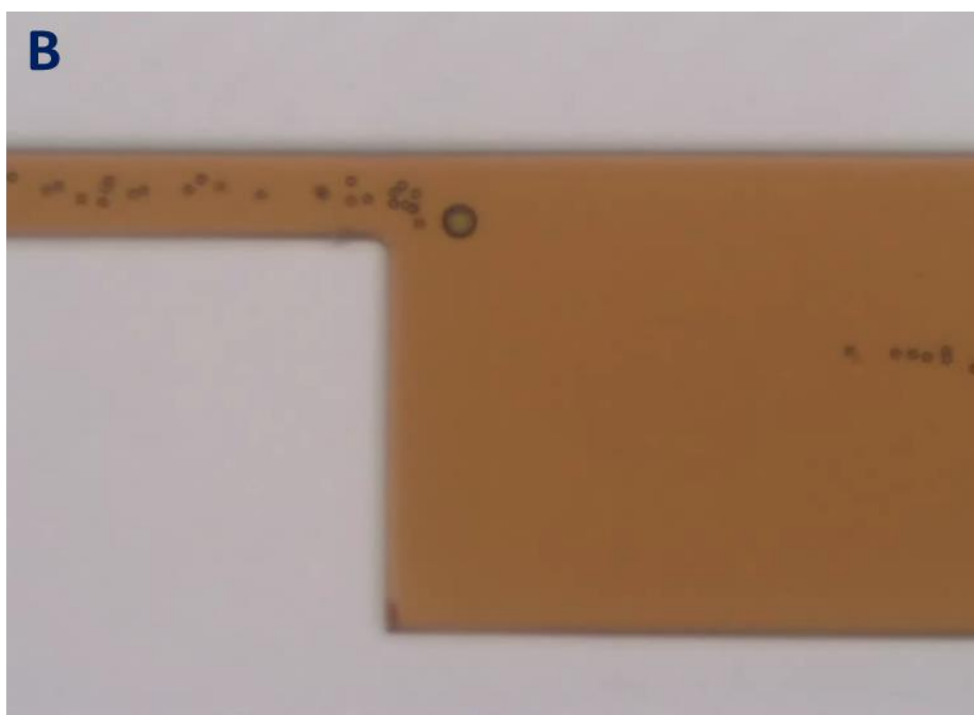
B

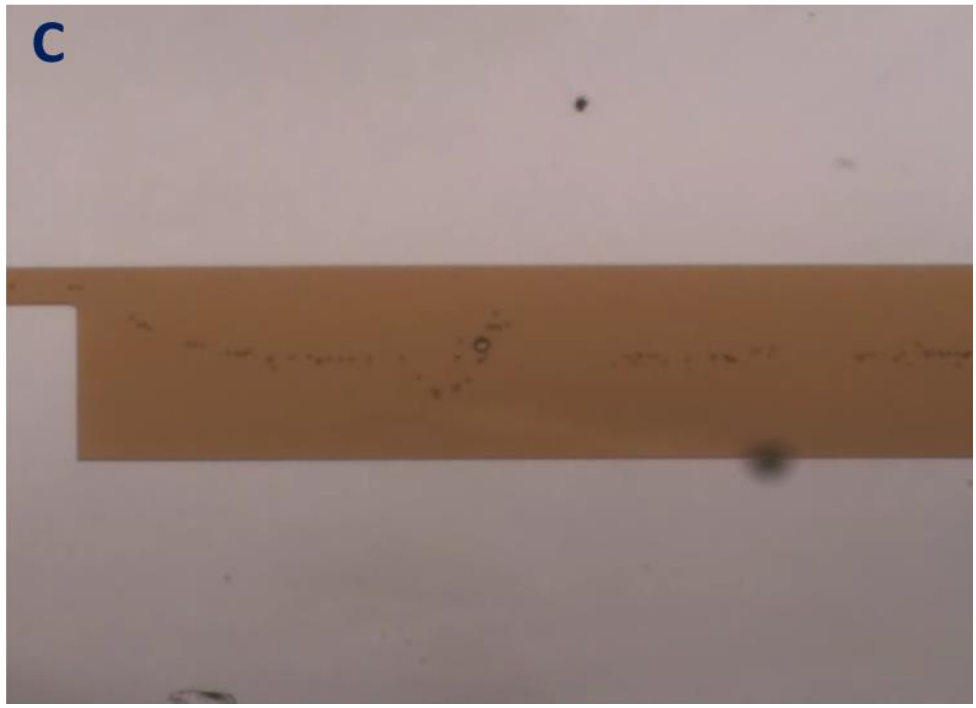
C

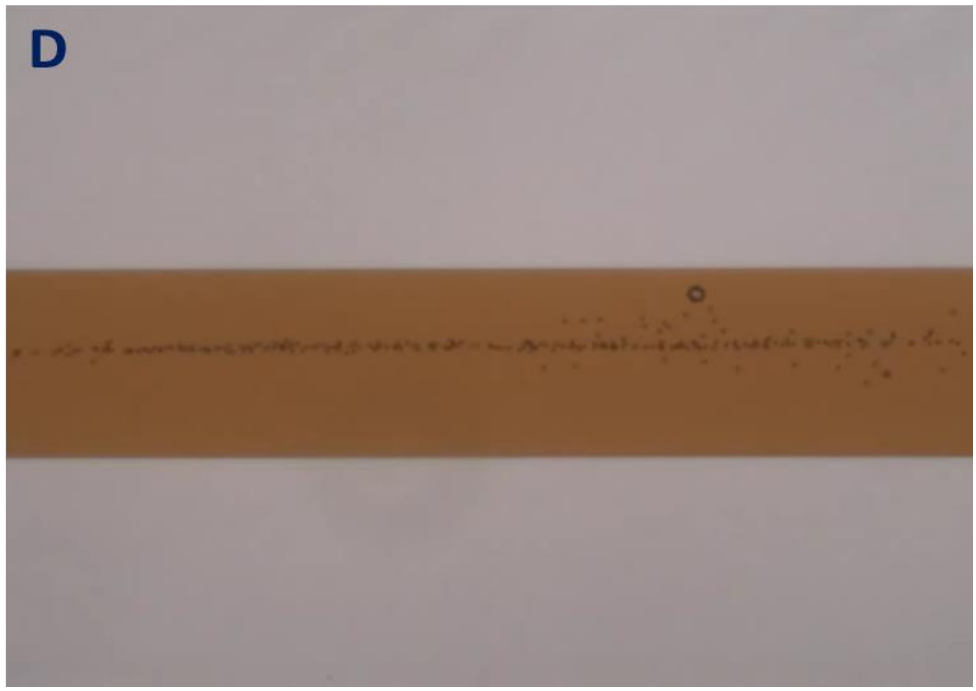
D

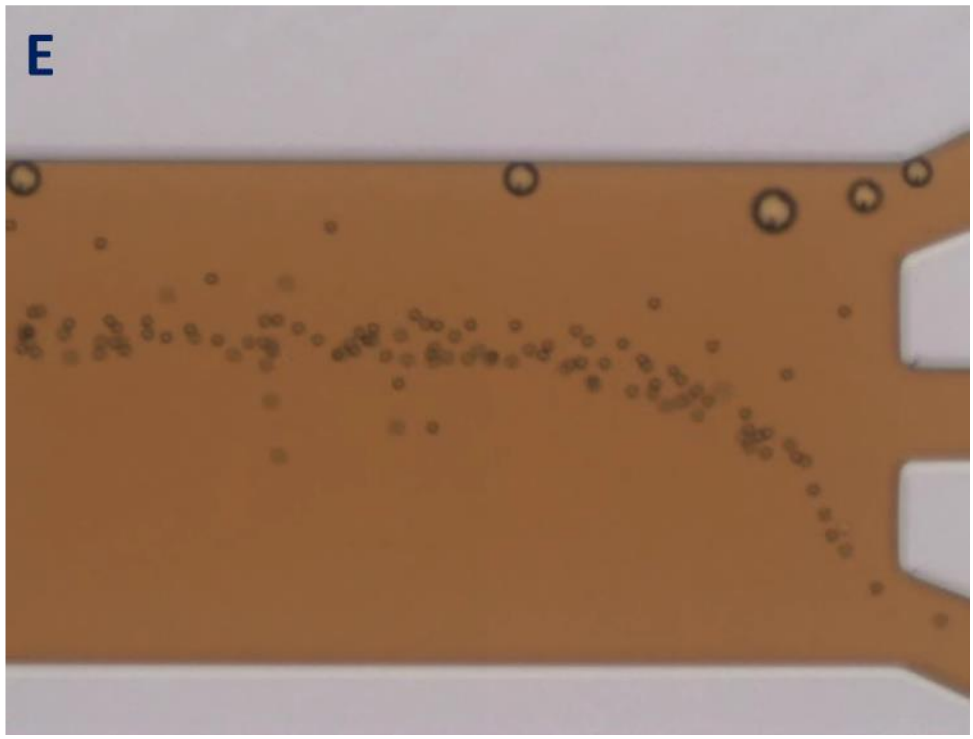
E

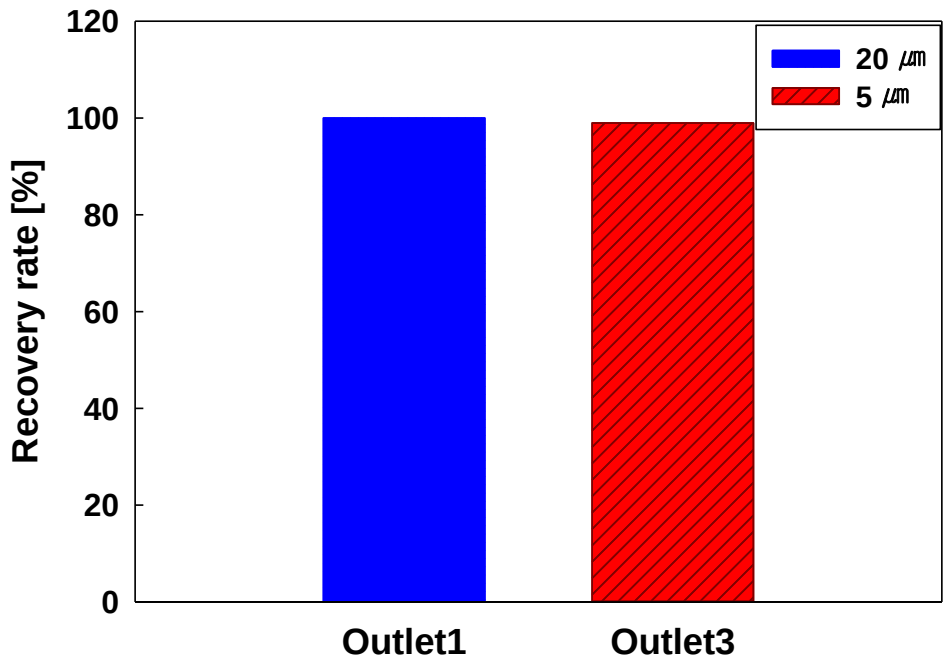

Figure 4.11. Recovery rate at each outlet for the collected polystyrene particles after the experiment. The recovery rate defines as the ratio of the total number of particles flew for 30 s to the number of the particles corresponding to each of the particle size flew for 30 s.

In addition, we observed other optimum experimental condition for the particle separation. A solution which consists PEO 0.5 wt% and 0.6 wt% in DI water mixed with glycerol solution containing ferrofluid 12.5 wt%, and 15 wt%, respectively, has a high purity size-based separation. We observed that if the concentration of PEO increases, the concentration of ferrofluid in solution also has to be increased for particle separation. Ferrofluid nanoparticles disturb particle focusing. Therefore adding ferrofluid makes various equilibrium position for diamagnetic particles (e.g. particle flows in the centerline or flows along the side wall of the channel) instead of one equilibrium position in this micro-scale separate system. More specifically, elasticity number at the expanding area is relatively small. Therefore, if particles have various equilibrium position in the particle focusing area, the particles also have various equilibrium position in the expanding channel. That is, particles flow through the expanding channel with their own position when they had at the position of the focusing area. If particles experience magnetophoretic repulsion force and get to separating by their size, the particles have to enter the expanding channel in a line. That is, it is critical that mixing between PEO and ferrofluid.

4.3. Analytical modeling : particle trajectory

Here we reported a behavior of particles for one fluid condition (PEO 0.4 wt% in DI water mixed with glycerol solution containing ferrofluid 10 wt% at the volume flow rates of 50 μlh^{-1}). The system for analytical model that we considered is illustrated in figure 4.12. We assume that the area is rectangular and the elastic force is negligible in this area (figure 4.4). We set a y-coordinate at the vertical centerline point of the channel. Therefore y has range of 0 to 125 μm. Therefore the distance between magnet and microchannel changes as 625 μm. Also we set a x-coordinate that particles are just about to experience magnetophoretic repulsion force at the expanding area. The system is a micro-scale, thus we assumed the magnetic field is strictly in the y direction. Applying the assumptions into the equation (6), equation (6) is changed as

$$H(y) = \frac{M_s}{\pi}\left[\tan^{-1}\left(\frac{(y+6.25\times10^{-4}+T)\sqrt{W^2+L^2+(y+6.25\times10^{-4}+T)^2}}{WL}\right) - \tan^{-1}\left(\frac{(y+6.25\times10^{-4})\sqrt{W^2+L^2+y^2}}{WL}\right)\right] \quad (25)$$

The parameters listed in table4.2 in our calculation. These parameters were chosen to match for the experimental conditions.

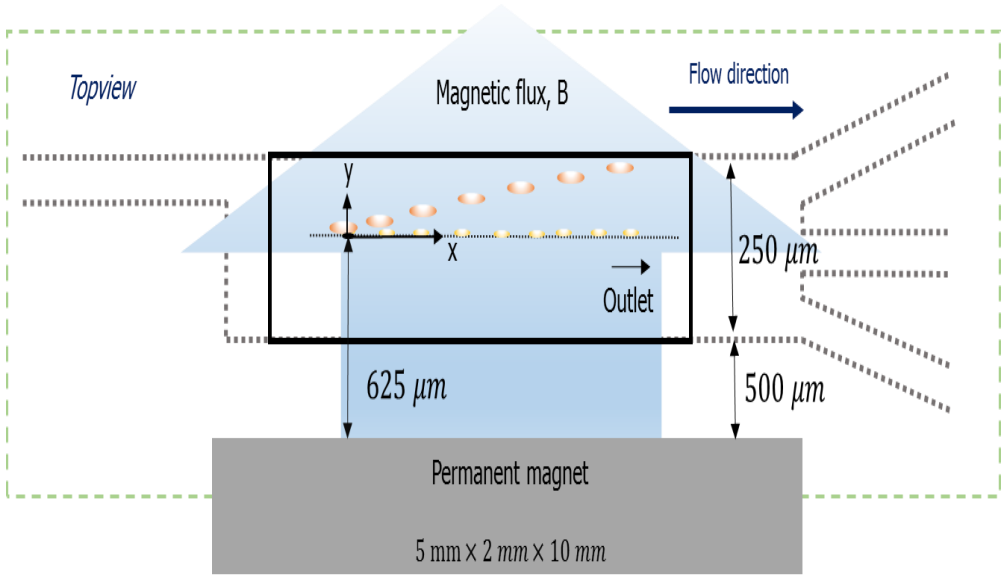

Figure 4.12. Analytical modeling area.

Table 4.2. Lists of parameters used in analytical modeling.

Parameter		Description	Value	unit
Magnet	B_s	Residual magnetic flux	0.198	T
	W	Magnet width	2×10^{-3}	m
	L	Magnet length	5×10^{-3}	m
	T	Thickness	1×10^{-2}	m
Solution	∅	Volume fraction of magnetic nanoparticles (original)	1.2	%
	η	Viscosity	0.00908	$\mathrm{Pa \cdot s}$
	M_d	Saturation moment of magnetic nanoparticles	4.377×10^5	$\mathrm{A/m}$
Diamagnetic particle	D_p	Particle diameter	5, 20	μm
	ρ	Density	1050	kg/m^3
Microchannel	w_c	Channel width	2.54×10^{-4}	m
	h_c	Channel length	5×10^{-5}	m
	Q	Volumetric flow rate	1.39×10^{-11}	m^3/s

Figure 4.13 and 4.14 demonstrate the particle position in y- direction over time for 5, 20 μm-particle, respectively. Velocity of the particle in y-direction obtained from the force balance equation (14). Particles are initially doing accelerated movement then switch to constant-speed movement.

For particle trajectories, we use equation (9) for x-direction particle velocity. We set an initial particle position as y=15 μm to match the experimental results. Y-coordinate is defined as 0 to 115 μm by the definition of the drag coefficient. Figure 4.15 shows the particle trajectory results during 0.75 seconds. The dark blue and dark red dot lines mean the theoretical results of 5, 20 μm particles, respectively. The blue and red triangle represent an experimental results of 5, 20 μm particles, respectively. This observation demonstrates that experimental results and theoretical results are matched each other. Therefore it depicts quadratic relations between velocity and the sizes of the particles.

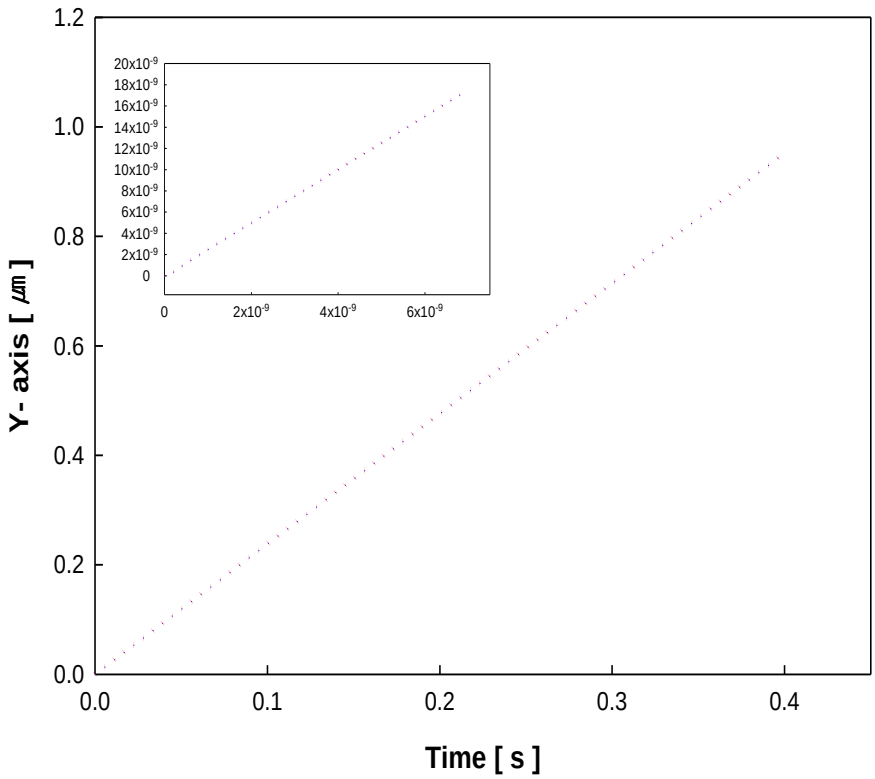

Figure 4.13. Time-dependent change in the position of y-axis in the case of the 5 μm particles.

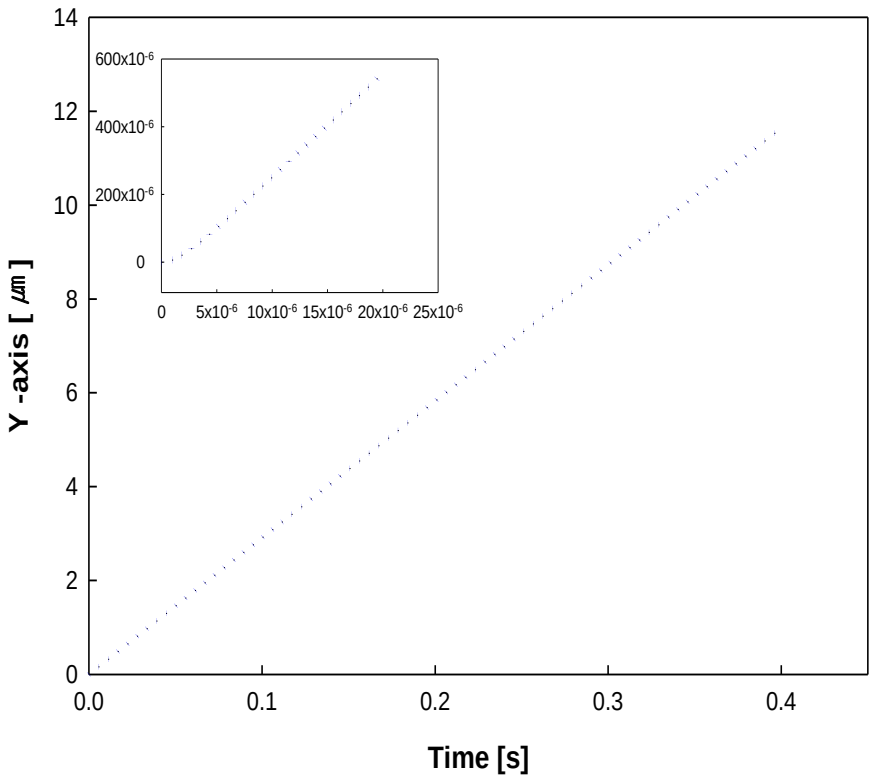

Figure 4.14. Time-dependent change in the position of y-axis in the case of the 20 μm particles.

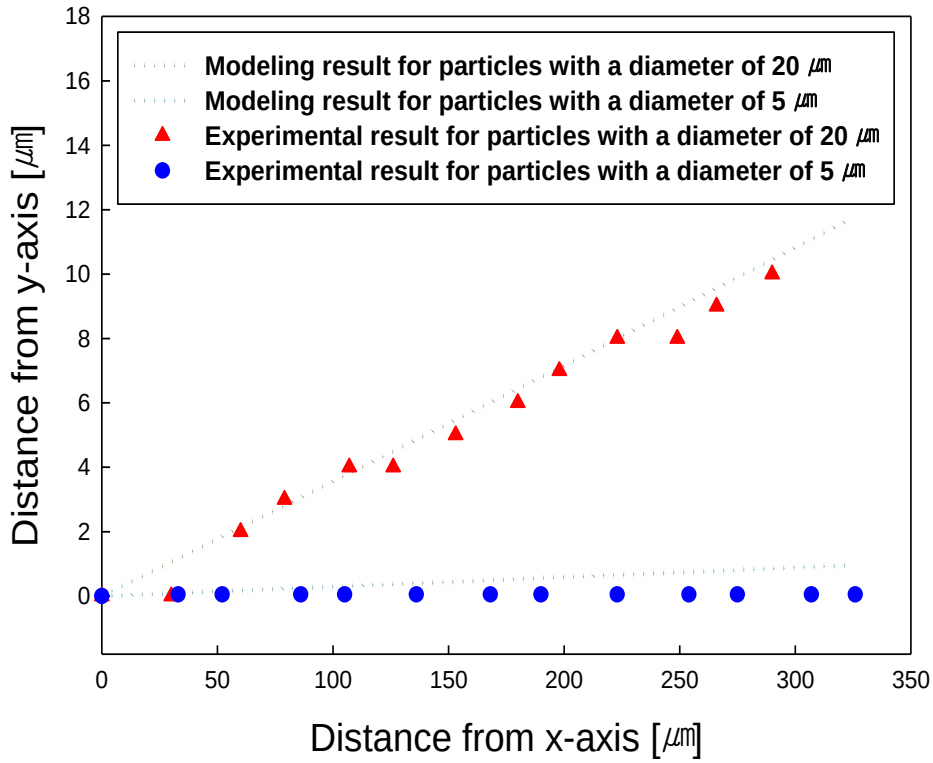

Figure 4.15. Experimental results of particle trajectories with a diameter of 5 μm and 20 μm particle, respectively. Analytical modeling of particle trajectories under the magnetic field with a diameter of 5 μm and 20 μm particle, respectively.

4.4. Numerical simulation

4.4.1. Governing equations

The area that we considered for numerical simulation is illustrated in figure 4.16 as dotted line. For setting the initial boundary condition of this region, we applied a behavior of the particles at the particle focusing region. Preceding research revealed that the particles have random position at the channel in Newtonian fluid and the particles align at the centerline of the channel in viscoelastic fluid [24]. Therefore we set an initial boundary condition for Newtonian fluid as; particles have random position at the channel. For viscoelastic fluid, we set an initial particle position of the centerline of the channel.

For the simulation, we sequentially solved the governing equations: (1) Maxwell equation, (2) momentum equation for creeping flow, and (3) particle dynamics. The governing equation of the magnetic field follows the Maxell equation. The continuity of magnetic flux is given by:

$$\nabla \cdot \mathbf{B} = 0 \tag{25}$$

Constitutive relation is also followed as:

$$\mathbf{B} = \mu_0 \mu_r \mathbf{H} \tag{26}$$

$$\mathbf{H} = -\nabla \mathbf{V_m}$$

Where μ_0, μ_r are free space permeability and relative permeability. Here we set the relative permeability as 1. **H** is a magnetic field vector and $\mathbf{V_m}$ is the magnetic scalar potential. We set the **H**=0 for an initial condition. Since the

Reynolds number in microfluidic channels is very small (less than ~1), the inertial effect is often negligible. As a result, the flow follows creeping flow. The momentum equation at the stationary condition we used as:

$$0 = \nabla \cdot [p\mathbf{I} + \mu(\nabla \mathbf{u} + (\nabla \mathbf{u})^{T}] + \mathbf{F} \tag{27}$$

Where **F** is an applied body force, $\mathbf{u}$ is fluid velocity, μ is fluid viscosity, and ρ is fluid density. The continuity equation is given by:

$$\rho(\nabla \cdot \mathbf{u}) = 0 \tag{28}$$

For the particle tracing, we set a force balancing equation for Stokes drag force and magnetophoretic force.

$$\frac{d(m_p \mathbf{v})}{dt} = \mathbf{F} = \mathbf{F_D} + \mathbf{F_M} \tag{29}$$

Where m_p is a mass of the particle and $\mathbf{v}$ is a particle velocity. **F** is a total body force. The drag force follows Stokes drag law.

$$\mathbf{F_D} = \frac{1}{\tau_p} m_p(\mathbf{u} - \mathbf{v}) \tag{30}$$

$$\tau_p = \frac{\rho_p d_p^2}{18\mu}$$

In which ρ_p is particle density and d_p is a particle diameter.

The magnetophoretic repulsion force is expressed as follows.

$$\mathbf{F_M} = 2\pi r_p^3 \mu_0 \mu_{r,f} k \nabla \mathbf{H}^2 \tag{31}$$

In which $\mu_{r,f}$ is fluid permeability, r_p is a particle diameter and k is the turbulent kinetic energy. Herein, we set no slip boundary condition and initial particle velocity.

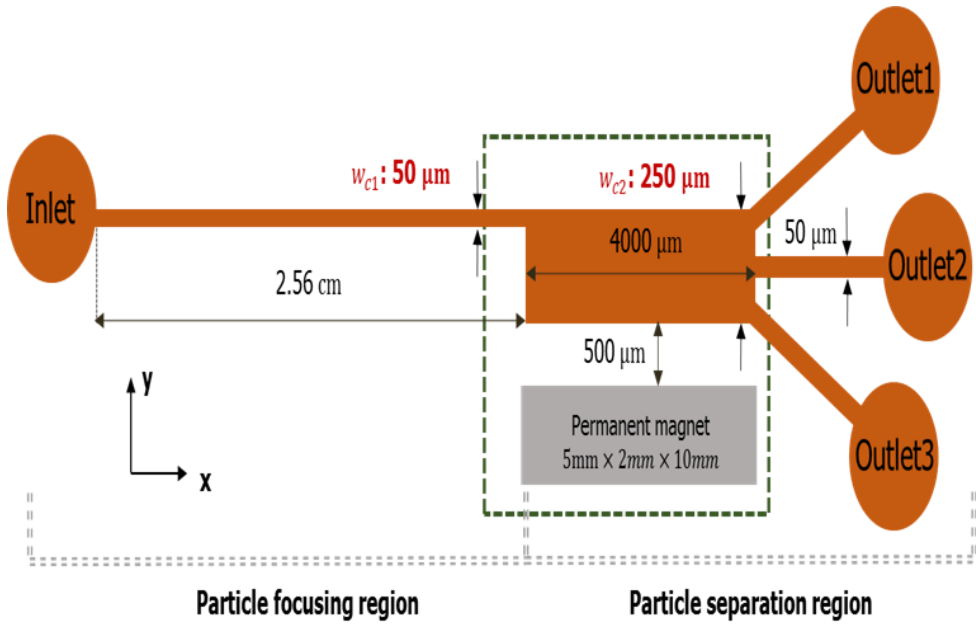

Figure 4.16. Illustration of simulation area.

4.4.2. Simulation results of size-based particle separation

Figure 4.17-20 demonstrate the behavior of the particles in Newtonian fluid under the magnetic field. Due to their initial boundary condition, two types of the particles randomly enter through the channel (figure 4.17 and 4.18). Under the magnetic field, particle experiences negative magnetophoresis by their size. However the particles have random position at the channel therefore they randomly move out and do not separate each other. As shown in figure 4.19 and 4.20.

Figure 4.21-24 show the behavior of the particles in viscoelastic fluid under the magnetic field. Figure 4.21 and 4.22 demonstrate that the 5, 20 μm particles are focused at the centerline of the channel due to the initial boundary condition. Under the magnetic field, the magnitude of the magnetophoretic repulsion force acting on the particles is different depending on the size. Therefore 20 μm particles experience larger negative magnetophoresis than that of the 5 μm particles. Thus, the particles with the diameter of 20 μm can move further and can be collected at an outlet1 (figure 4.23). On the other hand, particles with a diameter of 5 μm are collected at outlet2 (figure 4.24).

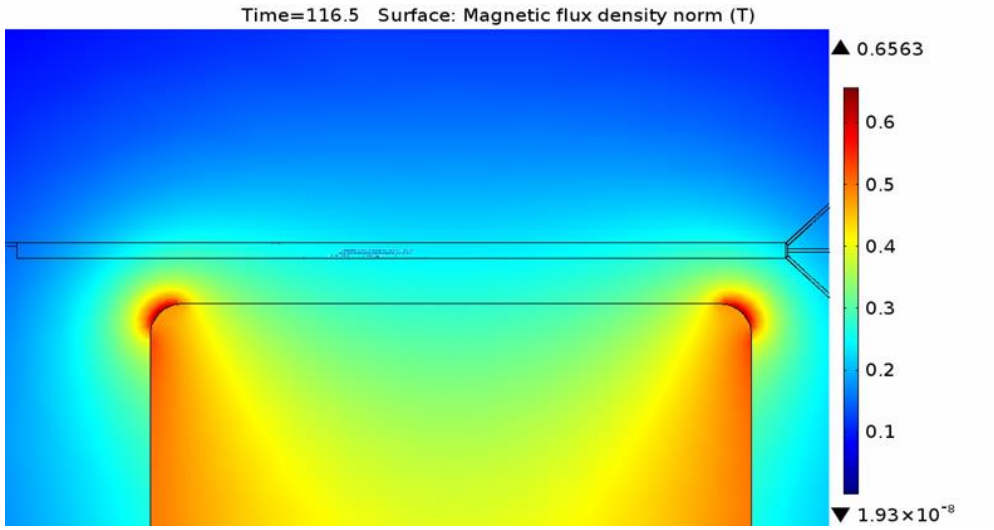

Figure 4.17. The image indicates of the migration of polystyrene particles in Newtonian fluid under the magnetic field. The image shows the distribution of 5 μm particles.

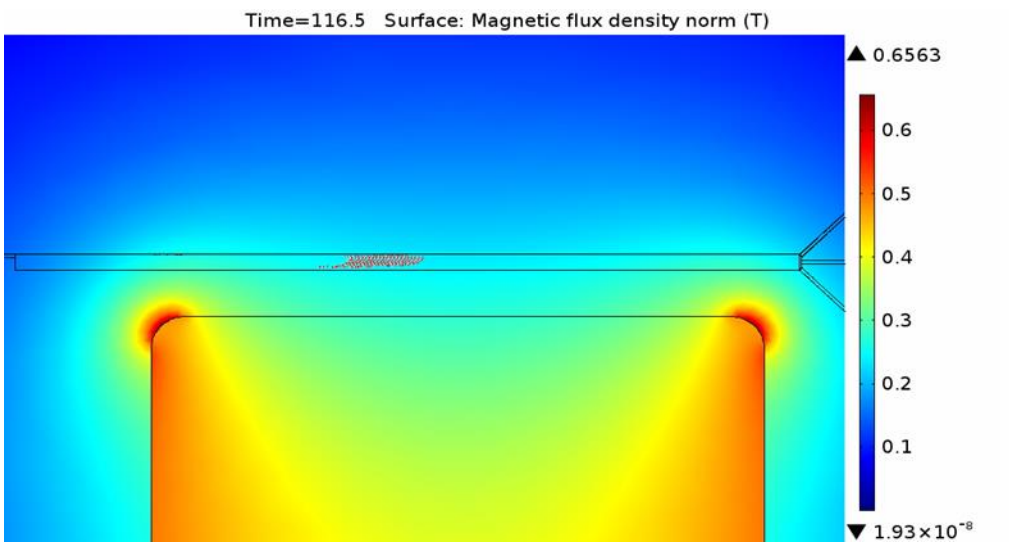

Figure 4.18. The image indicates of the migration of polystyrene particles in Newtonian fluid under the magnetic field. The image shows the distribution of 20 μm particles.

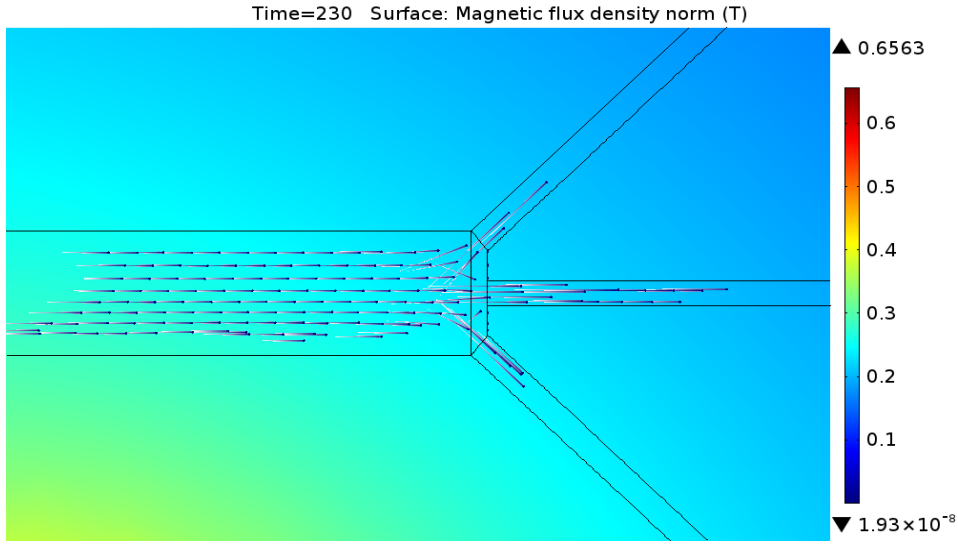

Figure 4.19. The image indicates of the migration of polystyrene particles in Newtonian fluid at the position of the outlet under the magnetic field. The image shows the distribution of 5 μm particles.

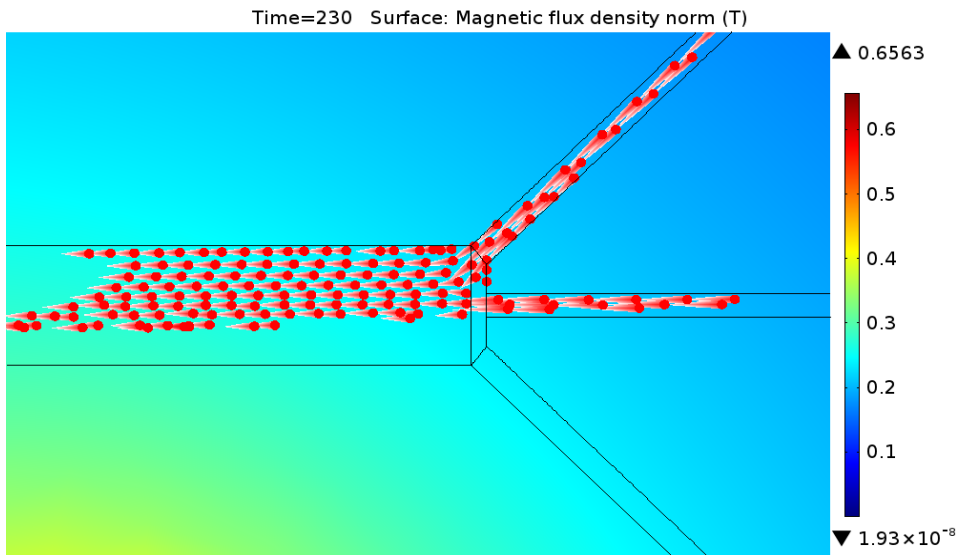

Figure 4.20. The image indicates of the migration of polystyrene particles in Newtonian fluid at the position of the outlet under the magnetic field. The image shows the distribution of 20 μm particles.

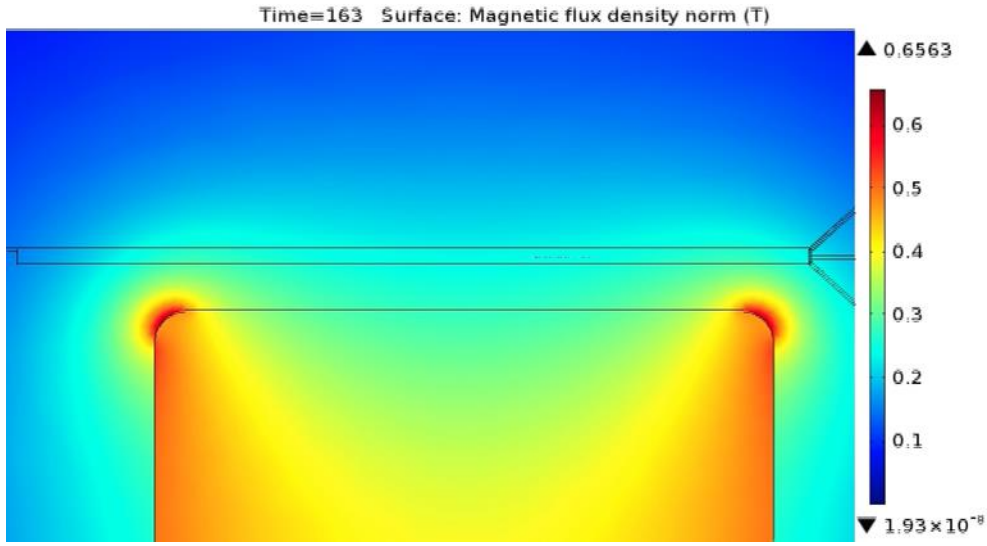

Figure 4.21. The image indicates of the migration of polystyrene particles in viscoelastic fluid under the magnetic field. The image shows the distribution of 5 μm particles.

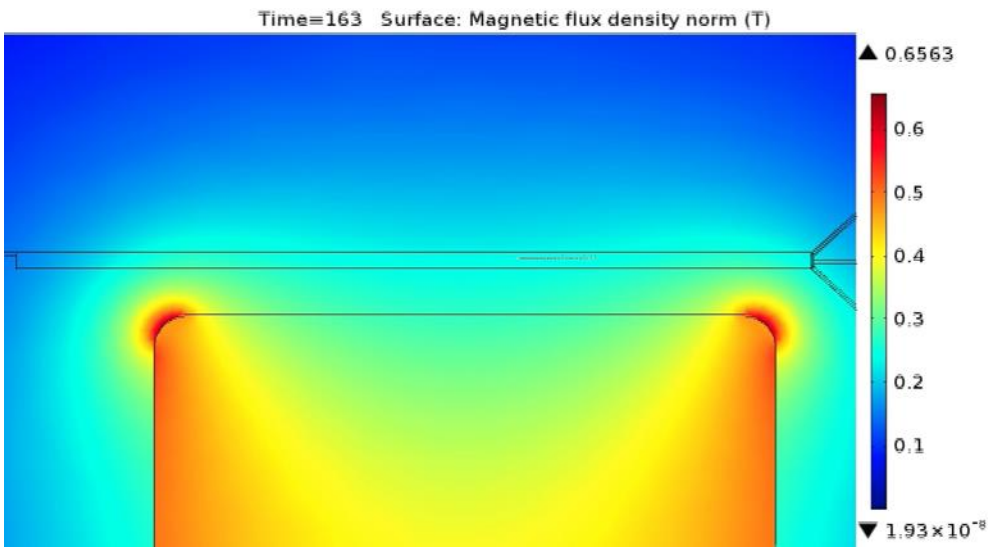

Figure 4.22. The image indicates of the migration of polystyrene particles in viscoelastic fluid under the magnetic field. The image shows the distribution of 20 μm particles.

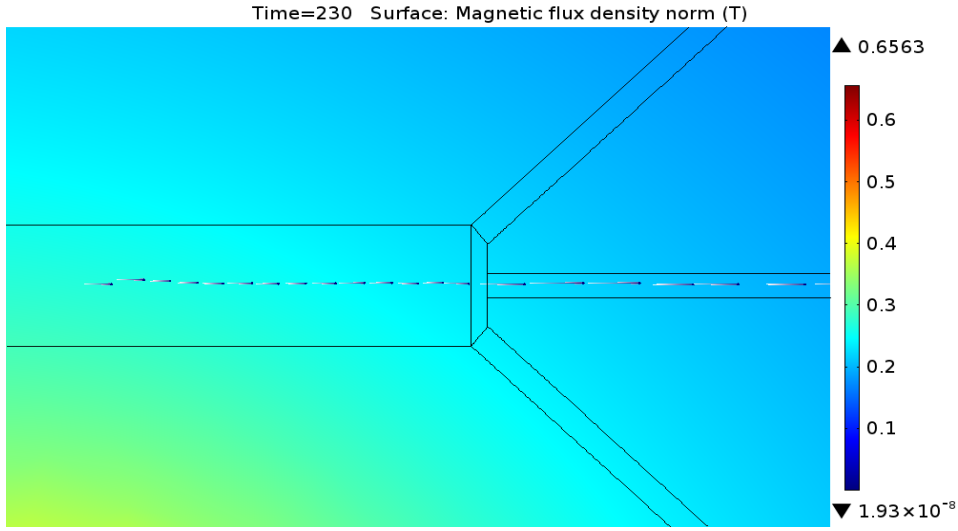

Figure 4.23. The image indicates of the migration of polystyrene particles in viscoelastic fluid at the position of the outlet under the magnetic field. The image shows the distribution of 5 μm particles.

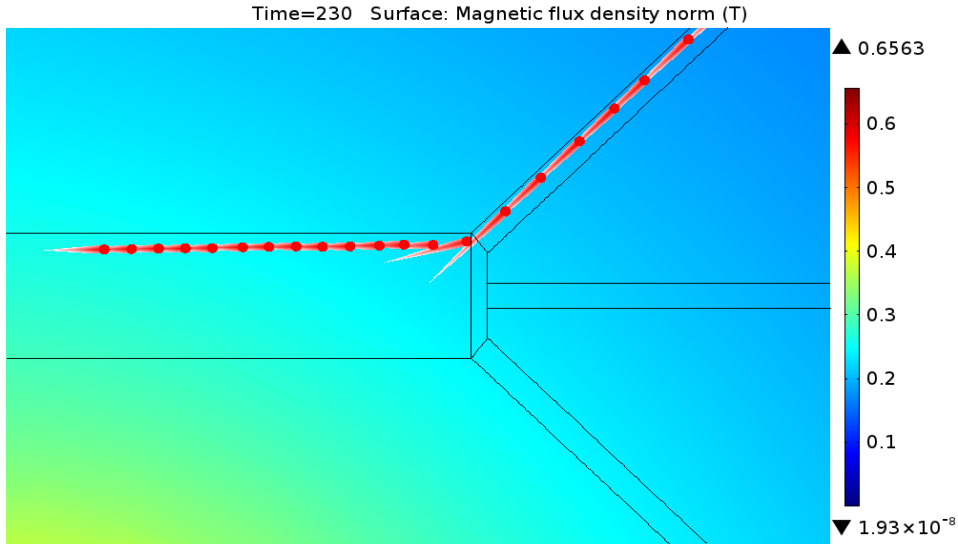

Figure 4.24. The image indicates of the migration of polystyrene particles in viscoelastic fluid at the position of the outlet under the magnetic field. The image shows the distribution of 20 μm particles.

IV.CONCLUSION

In conclusion, we developed a novel, active particle separation using elasto-inertial particle focusing and negative magnetophoresis. For viscoelastic fluid, two dimensionless quantities (Wi,Re) compete each other and make the particle alignment at the centerline of the channel. Permanent magnet produces non-uniform magnetic field that makes diamagnetic deflection in paramagnetic fluid.

In Newtonian fluid, particles experience negative magnetophoresis with a random positions in the expanding area (250 μm × 50 μm). Thus there was no size-based particle separation occur in this fluid condition. In viscoelastic fluid, particles enter through the expanding region with an alignment. Aligned particles can be effectively experienced magnetophoretic repulsion force by size. Thus, particles flow out to the different outlet by their size. 20 μm particles flowing along the side wall were collected through outlet1. In addition, 5 μm particles were collected through outlet 3. By adjusting the ratio of viscoelastic material and paramagnetic material, we found optimum conditions with a high recovery rate of particle separation conditions (more than 99.9%).

We developed an analytical modeling of particle trajectories in a microfluidic system under the magnetic field. We derived the equations of motion for particle using two dominant magnetic buoyancy and drag force. The results indicated that particles would be increasingly deflected when the size of the particles increased. A numerical simulation under the magnetic field carried out the particles behaviors of Newtonian and viscoelastic fluid, respectively. Simulation results indicated that deflection of the particle depends on their size and confirmed the necessity of using viscoelastic fluid for particle separation. Experimental results

confirmed the validity of the analytical modeling and numerical simulation results.

We envision that this study ultimately leads to improved performance of the microfluidic devices in a wide range of applications in medical diagnosis and label-free handling microbiological particle.

REFERENCES

[1] J. P. Nolan and L. A. Sklar, "The emergence of flow cytometry for sensitive, real-time measurements of molecular interactions," *Nature Biotechnology,* vol. 16, pp. 633-638, Jul 1998.

[2] X. H. Cheng, D. Irimia, M. Dixon, K. Sekine, U. Demirci, L. Zamir, *et al.*, "A microfluidic device for practical label-free CD4+T cell counting of HIV-infected subjects," *Lab on a Chip,* vol. 7, pp. 170-178, 2007.

[3] M. Antia, T. Herricks, and P. K. Rathod, "Microfluidic approaches to malaria pathogenesis," *Cellular Microbiology,* vol. 10, pp. 1968-1974, Oct 2008.

[4] P. Gascoyne, J. Satayavivad, and M. Ruchirawat, "Microfluidic approaches to malaria detection," *Acta Tropica,* vol. 89, pp. 357-369, Feb 2004.

[5] A. van de Stolpe, K. Pantel, S. Sleijfer, L. W. Terstappen, and J. M. J. den Toonder, "Circulating Tumor Cell Isolation and Diagnostics: Toward Routine Clinical Use," *Cancer Research,* vol. 71, pp. 5955-5960, Sep 15 2011.

[6] A. A. S. Bhagat, S. S. Kuntaegowdanahalli, and I. Papautsky, "Inertial microfluidics for continuous particle filtration and extraction," *Microfluidics and Nanofluidics,* vol. 7, pp. 217-226, Aug 2009.

[7] D. Di Carlo, D. Irimia, R. G. Tompkins, and M. Toner, "Continuous inertial focusing, ordering, and separation of particles in microchannels," *Proceedings of the National Academy of Sciences of the United States of America,* vol. 104, pp. 18892-18897, Nov 27 2007.

[8] S. A. Soper, K. Brown, A. Ellington, B. Frazier, G. Garcia-Manero, V. Gau,

et al., "Point-of-care biosensor systems for cancer diagnostics/prognostics," *Biosensors & Bioelectronics*, vol. 21, pp. 1932-1942, Apr 15 2006.

[9] A. J. Tudos, G. A. J. Besselink, and R. B. M. Schasfoort, "Trends in miniaturized total analysis systems for point-of-care testing in clinical chemistry," *Lab on a Chip*, vol. 1, pp. 83-95, 2001.

[10] H. W. Hou, A. A. S. Bhagat, A. G. L. Chong, P. Mao, K. S. W. Tan, J. Y. Han, *et al.*, "Deformability based cell margination-A simple microfluidic design for malaria-infected erythrocyte separation," *Lab on a Chip*, vol. 10, pp. 2605-2613, 2010.

[11] J. Nam, H. Lim, D. Kim, H. Jung, and S. Shin, "Continuous separation of microparticles in a microfluidic channel via the elasto-inertial effect of non-Newtonian fluid," *Lab on a Chip*, vol. 12, pp. 1347-1354, 2012.

[12] S. Miltenyi, W. Muller, W. Weichel, and A. Radbruch, "High-Gradient Magnetic Cell-Separation with Macs," *Cytometry*, vol. 11, pp. 231-238, 1990.

[13] T. T. Zhu, F. Marrero, and L. D. Mao, "Continuous separation of non-magnetic particles inside ferrofluids," *Microfluidics and Nanofluidics*, vol. 9, pp. 1003-1009, Oct 2010.

[14] A. Karimi, S. Yazdi, and A. M. Ardekani, "Hydrodynamic mechanisms of cell and particle trapping in microfluidics," *Biomicrofluidics*, vol. 7, Mar 2013.

[15] A. Higuchi and Y. Tsukamoto, "Cell separation of hepatocytes and fibroblasts through surface-modified polyurethane membranes," *Journal of Biomedical Materials Research Part A*, vol. 71A, pp. 470-479, Dec 1 2004.

[16] Y. Ito and K. Shinomiya, "A new continuous-flow cell separation method

based on cell density: Principle, apparatus, and preliminary application to separation of human buffy coat," *Journal of Clinical Apheresis,* vol. 16, pp. 186-191, 2001.

[17] K. W. Kwon, S. S. Choi, S. H. Lee, B. Kim, S. N. Lee, M. C. Park, *et al.*, "Label-free, microfluidic separation and enrichment of human breast cancer cells by adhesion difference{," *Lab on a Chip,* vol. 7, pp. 1461-1468, 2007.

[18] N. Pamme and A. Manz, "On-chip free-flow magnetophoresis: Continuous flow separation of magnetic particles and agglomerates," *Analytical Chemistry,* vol. 76, pp. 7250-7256, Dec 15 2004.

[19] R. Pethig, "Review Article-Dielectrophoresis: Status of the theory, technology, and applications," *Biomicrofluidics,* vol. 4, Jun 2010.

[20] L. T. Liang, S. Qian, and X. C. Xuan, "Three-dimensional electrokinetic particle focusing in a rectangular microchannel," *Journal of Colloid and Interface Science,* vol. 350, pp. 377-379, Oct 1 2010.

[21] T. Laurell, F. Petersson, and A. Nilsson, "Chip integrated strategies for acoustic separation and manipulation of cells and particles," *Chemical Society Reviews,* vol. 36, pp. 492-506, 2007.

[22] S. H. Cho, J. M. Godin, C. H. Chen, W. Qiao, H. Lee, and Y. H. Lo, "Review Article: Recent advancements in optofluidic flow cytometer," *Biomicrofluidics,* vol. 4, Dec 2010.

[23] S. Yang, J. Y. Kim, S. J. Lee, S. S. Lee, and J. M. Kim, "Sheathless elasto-inertial particle focusing and continuous separation in a straight rectangular microchannel," *Lab on a Chip,* vol. 11, pp. 266-273, 2011.

[24] D. J. Lee, H. Brenner, J. R. Youn, and Y. S. Song, "Multiplex Particle Focusing via Hydrodynamic Force in Viscoelastic Fluids," *Scientific Reports,* vol. 3, Nov 19 2013.

[25] R. E. Rosensweig, *Ferrohydrodynamics*. Cambridge ; New York: Cambridge University Press, 1985.

[26] A. Winkleman, K. L. Gudiksen, D. Ryan, G. M. Whitesides, D. Greenfield, and M. Prentiss, "A magnetic trap for living cells suspended in a paramagnetic buffer," *Applied Physics Letters*, vol. 85, pp. 2411-2413, Sep 20 2004.

[27] L. T. Liang and X. C. Xuan, "Continuous sheath-free magnetic separation of particles in a U-shaped microchannel," *Biomicrofluidics*, vol. 6, Dec 2012.

[28] J. Zeng, C. Chen, P. Vedantam, V. Brown, T. R. J. Tzeng, and X. C. Xuan, "Three-dimensional magnetic focusing of particles and cells in ferrofluid flow through a straight microchannel," *Journal of Micromechanics and Microengineering*, vol. 22, Oct 2012.

[29] L. T. Liang and X. C. Xuan, "Diamagnetic particle focusing using ferromicrofluidics with a single magnet," *Microfluidics and Nanofluidics*, vol. 13, pp. 637-643, Oct 2012.

[30] S. Caserta, G. D'Avino, F. Greco, S. Guido, and P. L. Maffettone, "Migration of a sphere in a viscoelastic fluid under planar shear flow: Experiments and numerical predictions," *Soft Matter*, vol. 7, pp. 1100-1106, 2011.

[31] B. P. Ho and L. G. Leal, "Migration of Rigid Spheres in a 2-Dimensional Unidirectional Shear-Flow of a 2nd-Order Fluid," *Journal of Fluid Mechanics*, vol. 76, pp. 783-799, 1976.

[32] A. M. Leshansky, A. Bransky, N. Korin, and U. Dinnar, "Tunable nonlinear viscoelastic "focusing" in a microfluidic device," *Physical Review Letters*, vol. 98, Jun 8 2007.

[33] G. Romeo, G. D'Avino, F. Greco, P. A. Netti, and P. L. Maffettone,

"Viscoelastic flow-focusing in microchannels: scaling properties of the particle radial distributions," *Lab on a Chip,* vol. 13, pp. 2802-2807, 2013.

[34] S. Yang, S. S. Lee, S. W. Ahn, K. Kang, W. Shim, G. Lee, *et al.*, "Deformability-selective particle entrainment and separation in a rectangular microchannel using medium viscoelasticity," *Soft Matter,* vol. 8, pp. 5011-5019, 2012.

[35] T. T. Zhu, D. J. Lichlyter, M. A. Haidekker, and L. D. Mao, "Analytical model of microfluidic transport of non-magnetic particles in ferrofluids under the influence of a permanent magnet," *Microfluidics and Nanofluidics,* vol. 10, pp. 1233-1245, Jun 2011.

[36] J. P. Liu, *Nanoscale magnetic materials and applications*. New York, NY: Springer Verlag, 2009.

[37] E. P. Furlani, *Permanent magnet and electromechanical devices : materials, analysis, and applications*. San Diego, Calif.: Academic, 2001.

[38] W. M. Deen, *Analysis of transport phenomena*. New York: Oxford University Press, 1998.

[39] J. Happel and H. Brenner, *Low Reynolds number hydrodynamics : with special applications to particulate media*, 1st pbk. ed. The Hague ; Boston Hingham, MA, USA: M. Nijhoff ; Distributed by Kluwer Boston, 1983.

[40] E. P. Furlani and Y. Sahoo, "Analytical model for the magnetic field and force in a magnetophoretic microsystem," *Journal of Physics D-Applied Physics,* vol. 39, pp. 1724-1732, May 7 2006.

[41] G. Segre and A. Silberberg, "Radial Particle Displacements in Poiseuille Flow of Suspensions," *Nature,* vol. 189, pp. 209-&, 1961.

[42] A. A. S. Bhagat, S. S. Kuntaegowdanahalli, and I. Papautsky, "Enhanced

particle filtration in straight microchannels using shear-modulated inertial migration," *Physics of Fluids,* vol. 20, Oct 2008.

[43] L. E. Rodd, T. P. Scott, D. V. Boger, J. J. Cooper-White, and G. H. McKinley, "The inertio-elastic planar entry flow of low-viscosity elastic fluids in micro-fabricated geometries," *Journal of Non-Newtonian Fluid Mechanics,* vol. 129, pp. 1-22, Aug 10 2005.

[44] A. Karnis and S. Mason, "Particle motions in sheared suspensions. XIX. Viscoelastic media," *Transactions of The Society of Rheology (1957-1977),* vol. 10, pp. 571-592, 1966.

[45] M. A. Tehrani, "An experimental study of particle migration in pipe flow of viscoelastic fluids," *Journal of Rheology,* vol. 40, pp. 1057-1077, Nov-Dec 1996.

[46] T. T. Zhu, R. Cheng, and L. D. Mao, "Focusing microparticles in a microfluidic channel with ferrofluids," *Microfluidics and Nanofluidics,* vol. 11, pp. 695-701, Dec 2011.

[47] K. A. Mirica, S. S. Shevkoplyas, S. T. Phillips, M. Gupta, and G. M. Whitesides, "Measuring Densities of Solids and Liquids Using Magnetic Levitation: Fundamentals," *Journal of the American Chemical Society,* vol. 131, pp. 10049-10058, Jul 29 2009.

[48] L. T. Liang, C. Zhang, and X. C. Xuan, "Enhanced separation of magnetic and diamagnetic particles in a dilute ferrofluid," *Applied Physics Letters,* vol. 102, Jun 10 2013.

[49] L. T. Liang, J. J. Zhu, and X. C. Xuan, "Three-dimensional diamagnetic particle deflection in ferrofluid microchannel flows," *Biomicrofluidics,* vol. 5, Sep 2011.

[50] L. E. Rodd, T. P. Scott, J. J. Cooper-White, and G. H. McKinley, "Capillary break-up rheometry of low-viscosity elastic fluids," *Applied*

Rheology, vol. 15, pp. 12-27, 2005.

[51] J. J. Cooper-White, J. E. Fagan, V. Tirtaatmadja, D. R. Lester, and D. V. Boger, "Drop formation dynamics of constant low-viscosity, elastic fluids," *Journal of Non-Newtonian Fluid Mechanics,* vol. 106, pp. 29-59, Aug 30 2002.

[52] K. W. Ebagninin, A. Benchabane, and K. Bekkour, "Rheological characterization of poly(ethylene oxide) solutions of different molecular weights," *Journal of Colloid and Interface Science,* vol. 336, pp. 360-367, Aug 1 2009.

[53] S. Odenbach, "Ferrofluids - magnetically controlled suspensions," *Colloids and Surfaces a-Physicochemical and Engineering Aspects,* vol. 217, pp. 171-178, Apr 28 2003.

[54] R. Cheng, T. Zhu, and L. Mao, "Three-dimensional and analytical modeling of microfluidic particle transport in magnetic fluids," *Microfluidics and Nanofluidics,* pp. 1-12, 2013.

[55] J. Zhu, L. Liang, and X. Xuan, "On-chip manipulation of nonmagnetic particles in paramagnetic solutions using embedded permanent magnets," *Microfluidics and nanofluidics,* vol. 12, pp. 65-73, 2012.

초록

미세입자를 크기 별로 분리하는 것은 산업 생산과 화학 그리고 생물 의학 연구에서 필수가 되었다. 본 연구에서는 “관성 –탄성 입자 집중 효과” 와 “음의 자기 영동”을 이용하여 미세채널에서 입자의 크기에 따른 분리를 성공적으로 수행하였다. 본 연구에서 중요한 결과로 확장 영역에서 (250 μm × 50 μm) 입자가 갖는 궤적을 알아보기 위해 (1) 해석적 방법을 이용하여 자기 부력과 항력을 계산하였고 (2) 운동방정식을 적용하여 층류 유동 하에서 입자의 속도를 유도하였다. 또한 유한요소법을 사용하여 자기장 하에서 뉴턴 유체와 점탄성 유체 안의 입자 거동을 연구하여 크기에 따른 입자분리가 가능함을 보였다. 그 결과, 점탄성 유체에서 입자의 크기에 따른 자기 부력과 항력의 차이를 통한 미세 유체 소자 내에서 크기에 따른 입자 분리가 가능함을 입증하였다. 본 연구에서 제시한 플랫폼과 분석 연구가 미세유체소자 내에서 입자 분리의 새로운 방법을 제공할 것으로 기대된다.

주요어: 입자 분리, 관성–탄성 입자 집중, 음의 자기영동, 자성유체, 점탄성 유체

학번: 2012–23138